

## Measurement and analysis of the excitation function for alpha-induced reactions on Ga and Sb isotopes

M. Ismail

Variable Energy Cyclotron Centre, Bidhan Nagar, Calcutta-700 064, India

(Received 6 July 1989)

Excitation functions for the reactions  $^{69}\text{Ga}(\alpha, xn)^{73-x}\text{As}$ ,  $^{69}\text{Ga}(\alpha, p3n)^{69}\text{Ge}$ ,  $^{69}\text{Ga}(\alpha, 2p4n)^{67}\text{Ga}$ ,  $^{71}\text{Ga}(\alpha, xn)^{75-x}\text{As}$ ,  $^{121}\text{Sb}(\alpha, xn)^{125-x}\text{I}$ ,  $^{121}\text{Sb}(\alpha, p3n)^{121}\text{Te}$ , and  $^{123}\text{Sb}(\alpha, xn)^{127-x}\text{I}$  were obtained from the measurements of the residual activity of stacked foils from threshold to 65 MeV. The excitation functions for the production of  $^{74}\text{As}$ ,  $^{72}\text{As}$ ,  $^{71}\text{As}$ ,  $^{69}\text{Ge}$ , and  $^{67}\text{Ga}$  from  $\alpha$ -induced reactions on Ga and  $^{126}\text{I}$ ,  $^{124}\text{I}$ ,  $^{123}\text{I}$ ,  $^{121}\text{I}$ , and  $^{121}\text{Te}$  from  $\alpha$ -induced reactions on Sb are presented. The experimental data are compared with calculations considering equilibrium as well as preequilibrium reaction mechanisms according to the hybrid model of Blann. The high-energy part of the excitation functions are dominated by the preequilibrium reaction mechanism. Calculations were done using the *a priori* calculational method of Blann. From the reactions  $^{71}\text{Ga}(\alpha, 3n)^{72}\text{As}$  and  $^{123}\text{Sb}(\alpha, 3n)^{124}\text{I}$ , an initial exciton number  $n_0 = 4$  ( $n_n = 2$ ,  $n_p = 2$ ,  $n_h = 0$ ) with the mean-free-path multiplier parameter  $k$  set to 2 has been deduced for both the targets. However, there are a few exceptions. The theory overestimates the cross section for the  $^{69}\text{Ga}(\alpha, 2p4n)^{67}\text{Ga}$  reaction whereas it underestimates the cross section for the  $^{121}\text{Sb}(\alpha, p3n)^{121}\text{Te}$  reaction and the high-energy tail of  $^{121}\text{Sb}(\alpha, 2n)^{123}\text{I}$  excitation function. For the  $(\alpha, 2p4n)$  reactions on Ga the discrepancy between theory and experiment may be attributed partly to a breakup of the  $\alpha$  particle and partly to much more complex reaction mechanisms, whereas for the  $^{121}\text{Sb}(\alpha, p3n)^{121}\text{Te}$  reaction two different reaction mechanisms may be attributed. The large discrepancy between theory and experiment for the reaction  $^{121}\text{Sb}(\alpha, 2n)^{123}\text{I}$  at the high-energy tail of the excitation function may be attributed to emission of more than one preequilibrium nucleon which the theory cannot account for at present. Barring these reactions we have found that the overall agreement between theory and experiment is reasonably good, taking the limitations of the theory into account.

### I. INTRODUCTION

Nuclear reactions induced by medium energy projectiles ( $\approx 10$ – $50$  MeV/nucleon) are interesting in view of preequilibrium and equilibrium deexcitation processes. The highly excited ( $\approx 40$ – $200$  MeV) nuclear system produced by the projectile bombardment decays first by emitting a number of fast nucleons at the preequilibrium stage and later on by evaporating low-energy nucleons (mostly neutrons in medium and heavy nuclei) at the equilibrium stage. The preequilibrium process has been investigated by several authors.<sup>1–6</sup> Excitation functions for equilibrium and preequilibrium reactions have been studied in  $(\alpha, xn)$  and  $(\alpha, pxn)$  reactions.<sup>7–11</sup> Theoretical calculations for the preequilibrium process have been carried out in terms of exciton models.<sup>3</sup> Several models<sup>1–6, 12–17</sup> have been proposed to explain the emission of energetic light particles by the equilibration process (preequilibrium emission) from the nuclear system excited at medium energies. Predictions from these models as to excitation functions and the energy spectra of the emitted particles compared well with the existing experimental data. This has prompted a continued interest in these models as tools both to predict cross sections for a number of practical purposes and to test the adequacy of the underlying physics. There are many data on inclusive energy spectra of light ejectiles<sup>6</sup> but the complimentary information on residual nucleus excitation functions is far

from abundant. Regarding alpha-induced reactions, the integral cross-section data exist only for a few target nuclei. The present work on alpha-induced reactions on the target nuclei  $^{69}\text{Ga}$ ,  $^{71}\text{Ga}$ ,  $^{121}\text{Sb}$ , and  $^{123}\text{Sb}$  is intended to supply mostly new data in the alpha energy range from 10.0 to 65.0 MeV.

This paper continues a series of reports on gross features of the interactions of intermediate energy light projectile with medium mass nuclei. The experiments have been performed at the Variable Energy Cyclotron Centre (VECC), Calcutta. In this paper several excitation functions for the reactions  $^{69}\text{Ga}(\alpha, xn)^{73-x}\text{As}$ ,  $^{69}\text{Ga}(\alpha, p3n)^{69}\text{Ge}$ ,  $^{69}\text{Ga}(\alpha, 2p4n)^{67}\text{Ga}$ ,  $^{71}\text{Ga}(\alpha, xn)^{75-x}\text{As}$ ,  $^{121}\text{Sb}(\alpha, xn)^{125-x}\text{I}$ ,  $^{121}\text{Sb}(\alpha, p3n)^{121}\text{Te}$ , and  $^{123}\text{Sb}(\alpha, xn)^{127-x}\text{I}$  measured by using the stacked foil technique are being presented. The excitation functions of the radioactive products observed in reactions contain some information about the mechanism of the interaction of the  $\alpha$  particles with Ga and Sb isotopes. In this work calculations in the framework of the equilibrium statistical model and preequilibrium model were performed and the results are compared with experimental excitation functions. Various reaction mechanisms are indicated as contributing to the production of the radioactive nuclei.

### II. EXPERIMENTAL PROCEDURE

Excitation functions for alpha-induced reaction on  $^{69}\text{Ga}$ ,  $^{71}\text{Ga}$ ,  $^{121}\text{Sb}$ , and  $^{123}\text{Sb}$  were determined using the

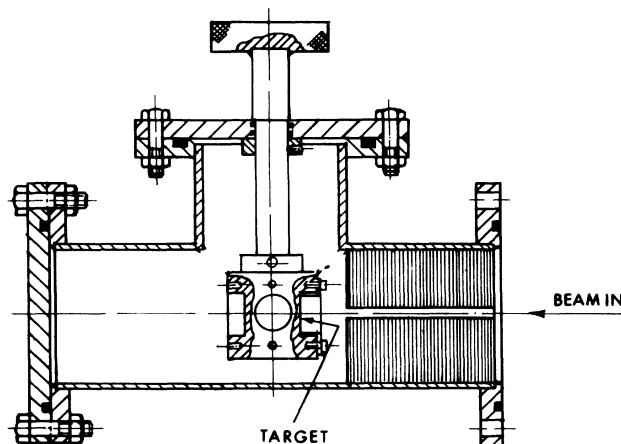
absolute yields of characteristic  $\gamma$  rays pertaining to the decay of each radioactive residual nuclide as usually done in the stacked foil technique (the details are presented below). The targets were obtained by vacuum evaporation of the gallium nitrate for Ga and antimony trioxide for Sb targets on 23.4  $\mu\text{m}$  thick Al backings (30 mm in diameter) placed over the masking plate. In the masking plate there were 16 open circles of 20 mm diameter. In one evaporation 16 targets were prepared. The thickness of the targets obtained after the evaporation was about  $\cong 1.0 \text{ mg/cm}^2$  for gallium and  $\cong 2.0 \text{ mg/cm}^2$  for antimony. The stacks were formed by placing alternatively 23.4  $\mu\text{m}$  aluminium foils (for alpha energies between 30.0 and 65.0 MeV) or 4.34  $\mu\text{m}$  aluminium foils (for alpha energies less than 30.0 MeV) as degraders of alpha energy over the targets. Then the stacks were irradiated in a chamber (as shown in Fig. 1) specially constructed for this purpose having the facility to irradiate four stacks one after another. The beam spot on the targets was limited to 5.0 mm in diameter by using a 10.0 cm long aluminium collimator in front of the targets. Each stack consists of about 15–20 targets. The stacks were exposed to the unanalysed external beam from the 224 cm variable energy cyclotron in Calcutta. The beam current on the targets was kept below 200 nA. The total  $\alpha$ -particle beam was collected and measured using a calibrated Ortec Current Integrator. In addition, from 23.4  $\mu\text{m}$  thick aluminium target backings and 23.4 or 4.34  $\mu\text{m}$  thick degraders, the absolute cross sections for the reaction  $^{27}\text{Al}(\alpha, 4p5n)^{22}\text{Na}$  and  $^{27}\text{Al}(\alpha, 4p3n)^{24}\text{Na}$  were also obtained from threshold to 65.0 MeV. However, the cross section for the production of  $^{22}\text{Na}$  and  $^{24}\text{Na}$  from Al are very well known.<sup>18</sup> By comparison of  $^{22}\text{Na}$  and  $^{24}\text{Na}$  production cross section from previous measurements and our measurements thus provides high reliability to the absolute cross-section measurements. The unanalysed beam energy resolution was  $\cong 0.2 \text{ MeV}$ . The accuracy in absolute energy is expected to be  $\cong 2.0 \text{ MeV}$ . However, for the excitation functions the energies are recalibrated with respect to thresholds of  $^{69}\text{Ga}(\alpha, 2n)^{71}\text{As}$  and  $^{121}\text{Sb}(\alpha, 4n)^{121}\text{I}$  reactions, i.e., to  $-15.15 \text{ MeV (c.m.)}$  and  $-33.19 \text{ MeV}$ , respectively.

In all of the irradiations the beam energy was degraded in the stacks at least by 20.0 MeV. The applicability of the stacked foil method due to the loss of beam intensity and contaminating background due to secondary reactions from the beam as it travels through a large amount of material is discussed below. The decrease in beam intensity  $\delta I_x$  as a function of the transversed foil thickness  $x$  (cm) is given by the expression

$$\delta I_x = I_0 [1.0 - \exp(-N\sigma x)] ,$$

assuming a constant reaction cross section  $\sigma$ . The quantity  $N$  (atoms/cm<sup>3</sup>) in the case of an element of atomic weight  $A$  and density  $\rho \text{ g/cm}^3$  is given by  $N = (\rho/A)N_0$ . For a compound of molecular weight  $M$  and density  $\rho$ , the quantity  $N$  is given as a summation of the  $N_i$  of atoms of the  $i$ th kind per cm<sup>3</sup>, i.e.,

$$N = \sum N_i = \sum (\rho N_0 / M) v_i ,$$



REACTION CHAMBER

FIG. 1. Target chamber.

where  $v_i$  is the number of atoms of the kind “ $i$ ” in a molecule of the compound and  $N_0$  is the Avogadro number ( $0.6022 \times 10^{24}$  atoms/mol). For  $\sigma = 2$  barns the maximum beam loss at the end of a high- $z$  stack is always  $\leq 0.3\%$  and hence can be neglected as shown in Ismail and Divatia.<sup>9,10</sup>

In reactions with the stack material the incoming beam will release a large amount of low-energy ( $E \leq 10 \text{ MeV}$ ) neutrons and protons which can further react with the targets in stacks and disturb the yield mainly through  $(n,p)$ ,  $(n,\alpha)$ ,  $(p,n)$ , and  $(p,\alpha)$  reactions. However, it was found by Ernst *et al.*<sup>11</sup> that the perturbative yields are mostly negligible.

The mean beam energy in each foil of a stacked foil assembly can be calculated from the energy degradation of the initial beam energy according to the given stopping power values for the different materials. We have used the stopping powers from the tabulated values of Williamson *et al.*<sup>19</sup> However, the tabulated values are in steps of 2.0 MeV up to 50.0 MeV and then in steps of 5.0 MeV thereafter. Therefore, interpolation is required at every foil of the stack. To improve the accuracy of interpolation the stopping powers are fitted by a nonlinear least-squares method to a function of the form

$$Y = \sum A_i X^{i-1} + \sum B_i \exp(-\lambda_i X) . \quad (1)$$

The fit improves the overall accuracy of the stopping-power interpolation. The average thickness of the degrader and backing foils was determined by weighing. Each foil was punched out into a circular shape having 30.0 mm in diameter. The target thickness was determined by weighing the backing before and after the evaporation.

The  $\gamma$  rays emitted by the activated foils were detected with a 114 cm<sup>3</sup> Ge(Li) detector (efficiency 30%) available at our centre (VECC). In most of the cases the  $\gamma$  rays, used in yield determination and listed in Tables I and II, stand out very prominently in the spectra and did not

TABLE I. Half-lives,  $\gamma$  energies, branching ratios of the  $\gamma$  decays, and  $Q$  values for  $\alpha$ -induced reactions on Ga and Al.

Nuclide	Half-lives	$E_\gamma$ (keV)	$I_\gamma$ (%) (abs)	Reaction	$Q$ values (keV)
$^{74}\text{As}$	17.78 d	596.0	60.2	$^{71}\text{Ga}(\alpha, n)^{74}\text{As}$	-4926.9
$^{72}\text{As}$	26.01 h	834.0	80.2	$^{71}\text{Ga}(\alpha, 3n)^{72}\text{As}$	-23 702.7
				$^{69}\text{Ga}(\alpha, n)^{72}\text{As}$	-6740.9
$^{71}\text{As}$	61.2 h	174.9	83.7	$^{71}\text{Ga}(\alpha, 4n)^{71}\text{As}$	-32 109.0
				$^{69}\text{Ga}(\alpha, 2n)^{71}\text{As}$	-15 147.3
$^{69}\text{Ge}$	39.05 h	574.0	11.74	$^{69}\text{Ga}(\alpha, p3n)^{69}\text{Ge}$	-31 303.7
		1106.0	27.3		
$^{67}\text{Ga}$	78.3 h	93.3	38.0	$^{69}\text{Ga}(\alpha, 2p4n)^{67}\text{Ga}$	-46 882.7
		184.6	23.7		
		300.2	19.0		
$^{24}\text{Na}$	14.96 h	1368.6	1.0	$^{27}\text{Al}(\alpha, 4p3n)^{24}\text{Na}$	-59 722.6
$^{22}\text{Na}$	2.602 yr	1275.5	0.999	$^{27}\text{Al}(\alpha, 4p5n)^{22}\text{Na}$	-79 100.3

pose any identification problem [as shown in Figs. 2(a) and 2(b)]. The  $\gamma$ -ray spectra from the Ge(Li) spectrometers were stored in 4096 channels of memory of a Canberra multichannel analyzer and were recorded on magnetic tapes. The ND-560 computer was used to analyze the  $\gamma$ -ray spectra stored on magnetic tapes. The program EXPANL1 was written to select the required peaks from the  $\gamma$ -ray spectra stored on magnetic tapes and prepare a File EXP2DT. Another program EXPANL2 was written to analyse the peaks stored in File EXP2DT as a combination of distorted Gaussians plus background terms

$$Y = \sum_{i=1,4} a_i X^{i-1} + \sum (A_k / \sqrt{2\pi}\sigma) \exp\{-0.5[(X - X_k)/\sigma]^2\} \times \{1.0 + 0.1P1[(X - X_k)/\sigma]^4 + 0.001P2[(X - X_k)/\sigma]^{12}\}, \quad (2)$$

where  $Y$  is the channel count and  $X$  is the channel number. The sum extends over the number of peaks to be fitted simultaneously. Its first term is pure Gaussian of area  $A$ , centroid  $X$  and full width at half maximum (FWHM)  $2.36\sigma$ . It is multiplied by a polynomial with terms to the 4th and 12th power whose coefficients are

$P1$  and  $P2$ . The program EXPANL2 is a modified version of the program written by J. Kern.<sup>20</sup> A detailed description of the properties of the above function was presented by J. Kern in Ref. 21. The above function fits the  $\gamma$ -ray spectra very well [as shown in Figs. 2(c) and 2(d)]; the integration of the analytical function as well as experimental peak was used for yield determination. The  $\gamma$ -ray yield was determined by integrating the experimental peak points and subtracting the calculated background from it, also shown in Figs. 2(c) and 2(d).

The efficiency calibrations of the detector were made with a standard  $^{152}\text{Eu}$  radioactive source available at our centre. The efficiency of the detector was interpolated to the required energy value from the measured efficiency curve. However, to improve the interpolation, the efficiency curve was similarly fitted by a nonlinear least-squares method to a function of the form given in Eq. (1). The fit improves the accuracy of interpolation considerably. The fit as shown in Fig 3 between experimental data and fitted function (solid line) is reasonably good.

The nuclear data necessary for the evaluation of the cross sections are presented in Tables I and II. The half-lives of the radioactive atoms are taken from the chart of nuclides; the  $\gamma$ -ray energies and branching ratios are taken from the table of isotopes.<sup>22</sup> In Tables I and II only those  $\gamma$  rays are listed which were chosen for the calcula-

TABLE II. Half-lives,  $\gamma$  energies, branching ratios of the  $\gamma$  decays, and  $Q$ -values for  $\alpha$ -induced reactions on Sb.

Nuclide	Half-lives	$E_\gamma$ (keV)	$I_\gamma$ (%) (abs)	Reaction	$Q$ values (keV)
$^{126}\text{I}$	13.0 d	388.6	0.35	$^{123}\text{Sb}(\alpha, n)^{126}\text{I}$	-6957.4
$^{124}\text{I}$	4.15 d	602.7	0.615	$^{123}\text{Sb}(\alpha, 3n)^{124}\text{I}$	-23 044.0
				$^{121}\text{Sb}(\alpha, n)^{124}\text{I}$	-7869.0
$^{123}\text{I}$	13.02 h	159.0	0.829	$^{123}\text{Sb}(\alpha, 4n)^{123}\text{I}$	-31 144.5
				$^{121}\text{Sb}(\alpha, 2n)^{123}\text{I}$	-15 369.5
$^{121}\text{I}$	2.12 h	212.2	0.84	$^{121}\text{Sb}(\alpha, 4n)^{121}\text{I}$	-33 186.3
$^{121}\text{Te}$	16.78 d	573.0	0.803	$^{121}\text{Sb}(\alpha, p3n)^{121}\text{Te}$	-30 127.0

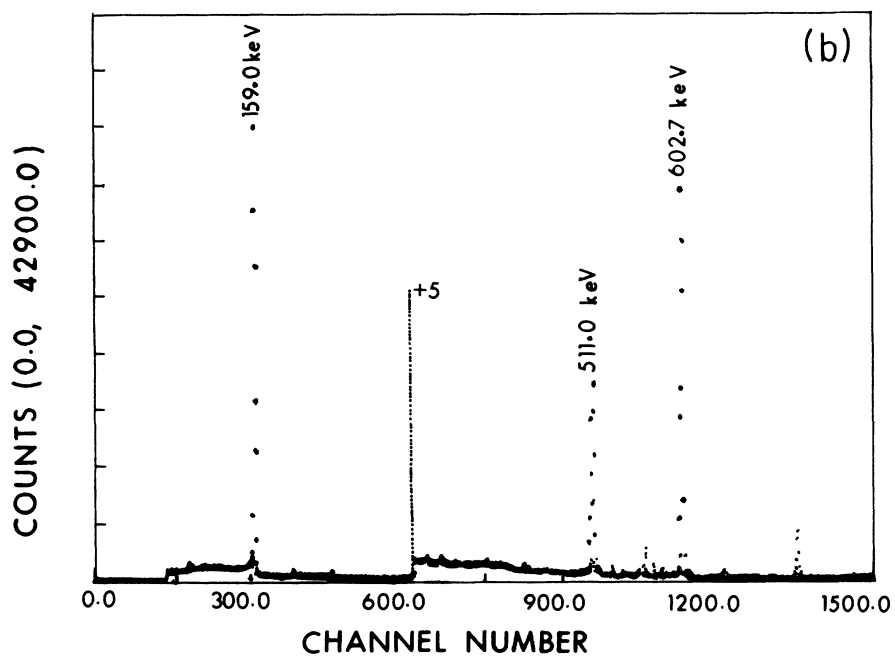
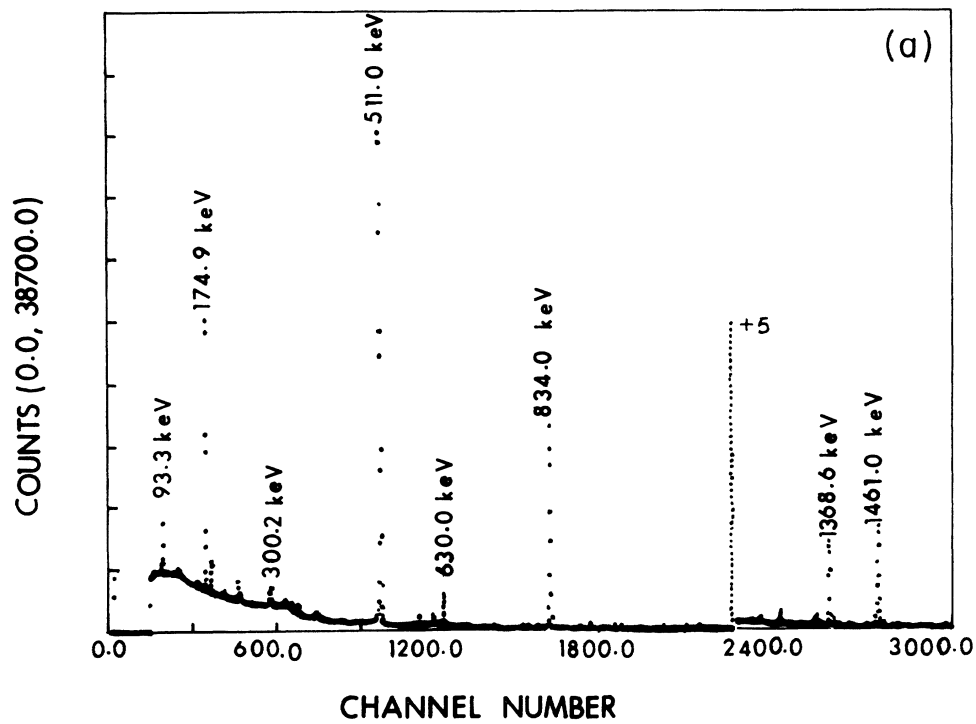


FIG. 2. (a) and (b) the  $\gamma$ -ray spectrum for  $\alpha$ -induced reaction on Ga taken at  $E_\alpha = 20.0$  MeV and on Sb, respectively. (c) The 834.0 keV peak fitted to the function of Eq. (2). Symbols + = experimental points, solid line is the fitted curve, and dot-dashed curve = calculated background. (d) Same as (c) but for a double peak.

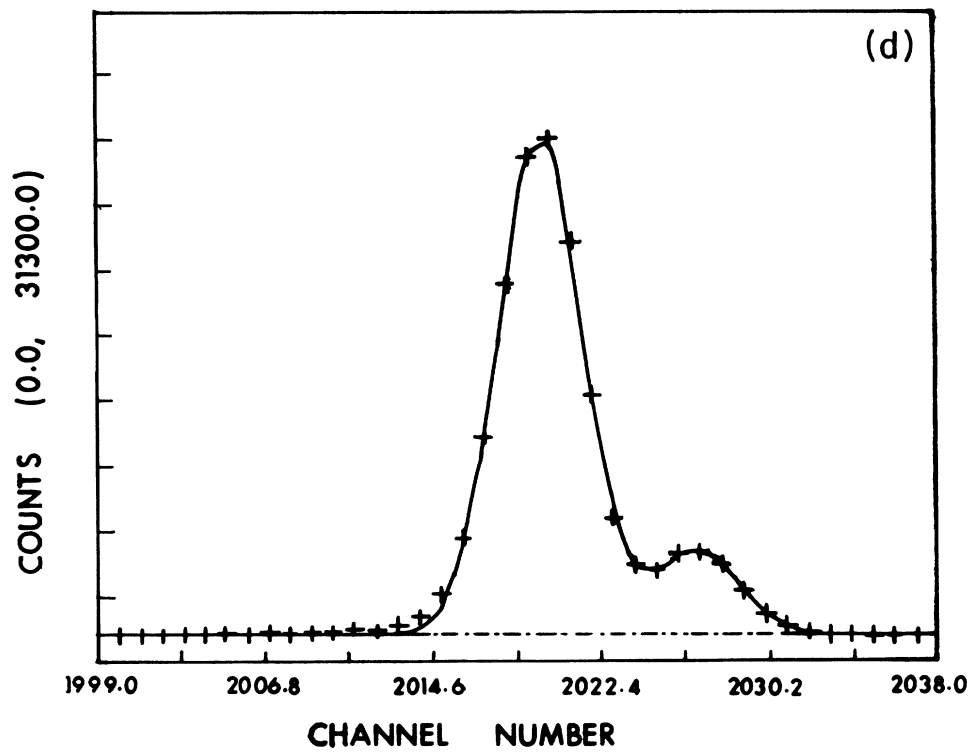
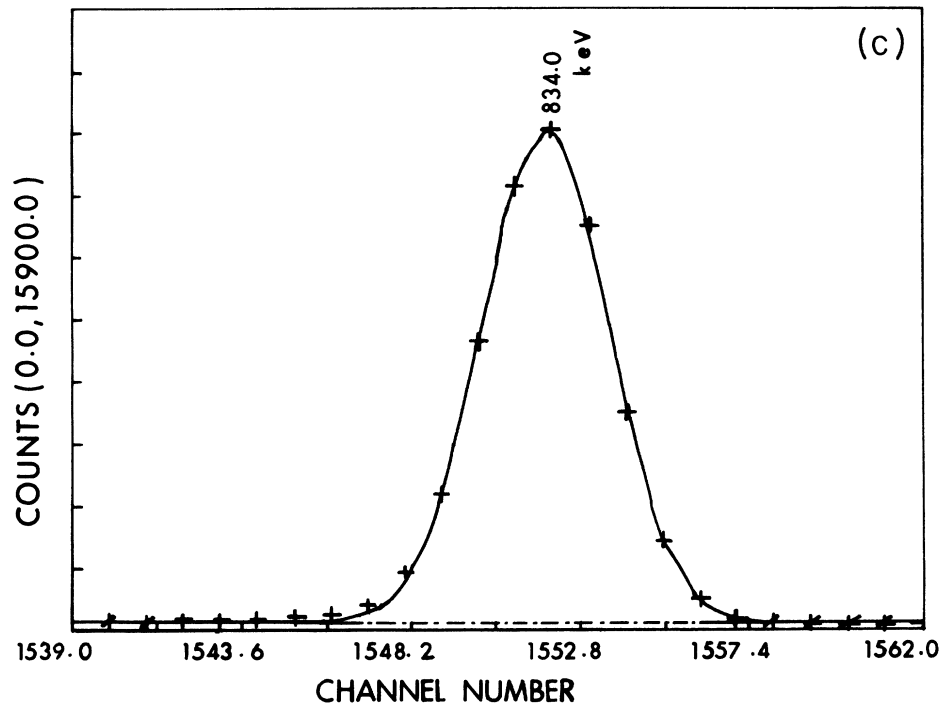


FIG. 2. (Continued).

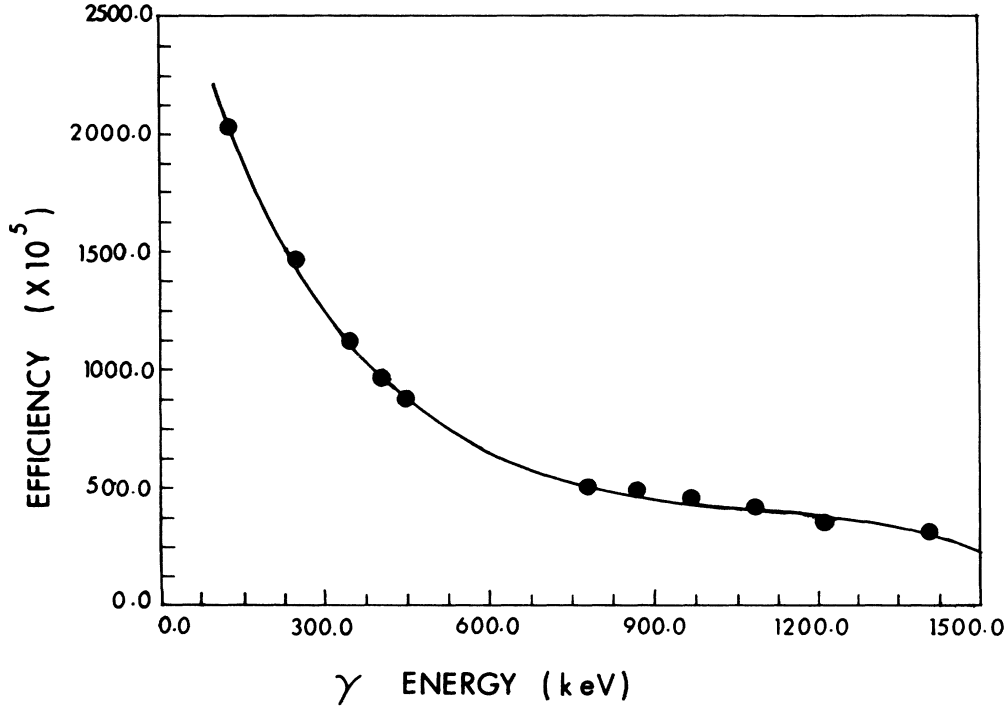


FIG. 3. Nonlinear least-squares fitted efficiency curve (solid line) as a function of  $\gamma$ -ray energy for the Ge(Li)  $\gamma$ -ray detector along with experimental points (● symbols).

tion of the cross sections. Also included in Tables I and II are reaction  $Q$  values which, however, exclude cluster emission. Thus in the case of  $\alpha$  emission 28.3 MeV will have to be added to the listed  $Q$  values.  $Q$  values were calculated by using the atomic mass table of Wapstra and Audi.<sup>23</sup>

#### A. Cross-section determination

The number of observed decays  $y(t)$  is related to the total number of decays  $z(t)$  during the measuring time  $t$  by

$$z(t) = y(t) / [\varepsilon(E_\gamma) I_\gamma(\text{abs})],$$

where  $\varepsilon(E)$  is the detector efficiency and  $I_\gamma(\text{abs})$  is the absolute  $\gamma$ -ray abundance (yield) per decay. The corresponding reaction yield  $N_0$  is given for simple decays (simple decays correspond to direct production of radio isotopes by the nuclear reactions and we have used only such decays in all the measurements reported here) by

$$N_0 = z(t) \exp(\lambda t_2) / \{ [1 - \exp(-\lambda t)] \times [1 - \exp(-\lambda t_1)] / \lambda t_1 \},$$

where  $\lambda = \ln 2 / T_{1/2}$  is the decay constant and  $t_1$  and  $t_2$  are the length of the irradiation time and the time between the end of the irradiation and the beginning of the measurement, respectively. In the cases where  $T_{1/2} \gg t_1, t_2$  the above relation becomes

$$N_0 = z(t) \exp(\lambda t_2) / \lambda t,$$

where  $N_0$  is related to the cross section  $\sigma$  by the relation

$$N_0 = \sigma (N_A \delta x) I,$$

where  $N_A$  is the number of atoms/cm<sup>3</sup> of the target material,  $\delta x$  is the thickness of the foil (in cm), and  $I$  is the total number of alpha beam particles used for the irradiation (integrated).

### III. EXPERIMENTAL RESULTS

#### A. Experimental error

In Tables III, IV, V, and VI the experimental cross sections for the reaction  $^{69}\text{Ga}(\alpha, xnyp)$ ,  $^{71}\text{Ga}(\alpha, xn)^{75-x}\text{As}$ ,  $^{121}\text{Sb}(\alpha, xnyp)$ , and  $^{123}\text{Sb}(\alpha, xn)^{127-x}\text{I}$  are presented, respectively, along with absolute errors. The absolute error consist of uncertainties due to target-foil thickness ( $\pm 1\%$ ), the beam current integration ( $\pm 1\%$ ), the detector efficiency ( $\pm 5\%$ ), and the analysis of the  $\gamma$ -ray spectra (statistical uncertainty), generally ( $\leq 2\%$ ). The uncertainties caused by the large size of the irradiation area and the nonuniformities of the target contribute about 5% to the average error of the cross section. However, the above-mentioned average error values do not include the uncertainties of the nuclear data used in the analysis.

**B. Integral excitation function  
for  $\alpha$ -induced reaction on  $^{69}\text{Ga}$**

In Table III and Figs. 4–7 our experimental results for the production of  $^{71}\text{As}$ ,  $^{72}\text{As}$ ,  $^{69}\text{Ge}$ , and  $^{67}\text{Ga}$  radionuclides via  $\alpha$ -induced reaction on  $^{69}\text{Ga}$  are summarized. The uncertainty given for the energy values includes those of target thickness and beam energy resolution ( $\pm 0.2$  MeV) only. Since the radionuclides  $^{71}\text{As}$  and  $^{72}\text{As}$

could also be produced via  $(\alpha, 4n)$  and  $(\alpha, 3n)$  reactions on  $^{71}\text{Ga}$ , respectively, in the overlapping region these cross sections are taken as proportional to their theoretical values based on the hybrid model of Blann.<sup>24</sup> These points are marked with symbol(\*) in Tables III and IV. The cross sections are in millibarns and the uncertainties are  $< 8\%$ . Since no data exist in the literature for  $\alpha$ -induced reactions on  $^{69}\text{Ga}$ , therefore, no comparison could be made with other measurements.

TABLE III. Experimental cross section for the  $\alpha$ -induced reaction on  $^{69}\text{Ga}$ .

$E$ (MeV)	$^{69}\text{Ga}(\alpha, n)^{72}\text{As}$ (mb)	$^{69}\text{Ga}(\alpha, 2n)^{71}\text{As}$ (mb)	$^{69}\text{Ga}(\alpha, 2p4n)^{67}\text{Ga}$ (mb)	$^{69}\text{Ga}(\alpha, p3n)^{69}\text{Ge}$ (mb)
10.10±0.25	47.5±3.8			
12.36±0.25	368.7±29.5			
14.42±0.25	647.4±51.8			
16.33±0.25	763.8±61.1	16.0±1.3		
18.06±0.24	787.0±63.0	146.8±11.7		
19.76±0.24	535.5±42.8	346.7±27.7		
21.33±0.23	327.0±26.2	531.3±42.5		
22.85±0.23	205.6±16.4	677.9±54.2		
24.28±0.23	133.2±10.7	798.4±63.9		
25.68±0.23	100.9±8.1	924.3±73.9		
27.01±0.23	98.8±7.9	845.8±67.7		
28.30±0.22	73.8±5.9 *	795.2±63.6		
29.56±0.22	77.8±6.2 *	802.9±64.2		
31.50±0.22	41.9±3.4 *	655.7±52.5		
33.44±0.22		519.8±41.6		
34.54±0.22			12.4±1.0	
35.33±0.22		362.2±29.0		
35.52±0.22		363.9±29.1		
36.46±0.22			29.0±2.3	
37.12±0.21		264.6±21.1		
37.37±0.21		251.2±20.1		
38.31±0.21			53.0±4.2	
39.16±0.21		204.4±16.4		
40.09±0.21			71.0±5.7	
40.90±0.21		173.4±13.9		
41.82±0.21			96.9±7.8	
42.59±0.21		142.5±11.4		
43.50±0.21			110.5±8.8	34.3±2.48
44.23±0.21		140.1±11.2*		
45.13±0.21			119.0±9.5	57.1±5.0
45.82±0.21		110.8±8.9*		
46.71±0.21			121.9±9.5	79.4±7.5
47.37±0.21		91.2±7.3*		
48.25±0.21			125.9±10.1	149.5±11.7
48.88±0.21		74.0±5.9*		
49.76±0.21			128.4±10.3	206.3±17.0
51.23±0.21			116.9±9.4	232.0±18.2
52.67±0.21			103.4±8.3	265.7±22.15
54.08±0.21			98.6±7.9	328.0±25.5
55.46±0.21				326.6±25.8
56.81±0.21			84.6±6.8	363.0±29.7
58.14±0.21			85.7±6.9	355.6±28.7
59.44±0.21			81.0±6.5	354.7±28.7
60.71±0.20			77.5±6.2	380.6±30.7
61.96±0.20			80.9±6.5	377.6±29.9
63.20±0.20			66.1±5.2	356.5±27.5
64.42±0.20			75.4±6.0	348.3±26.7

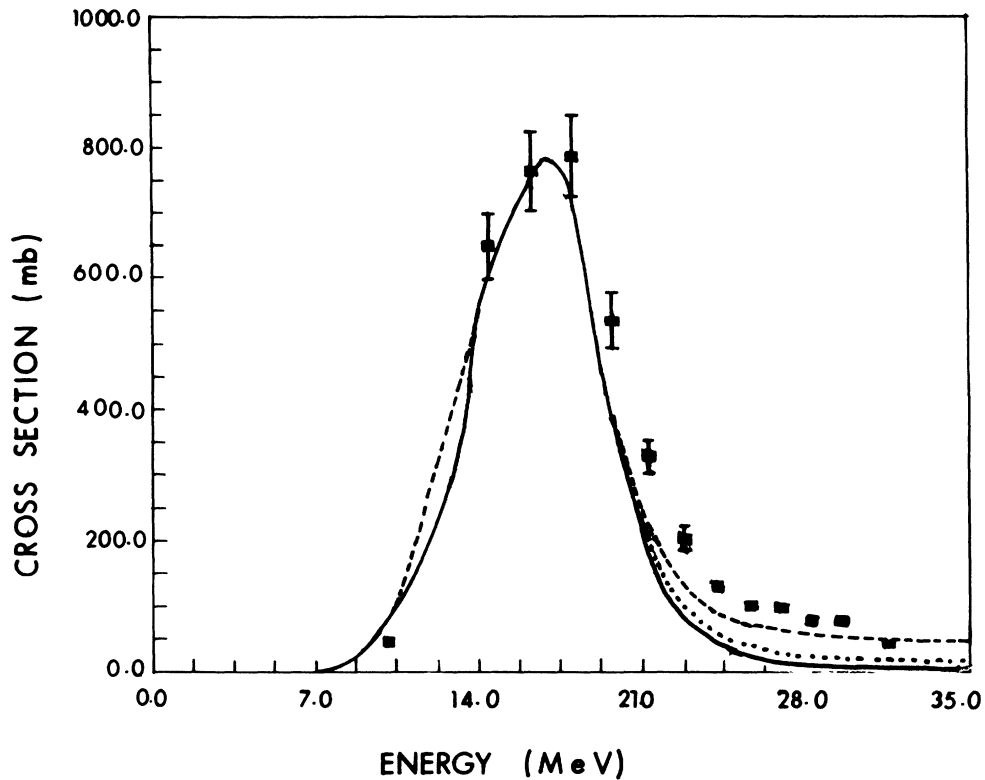


FIG. 4. The total residual production cross section in mb for the reaction  $^{69}\text{Ga}(\alpha, n)^{72}\text{As}$  (■ symbols) is plotted as a function of  $\alpha$ -particle bombarding energy. Solid line is the hybrid model calculation with  $n_o=4$  ( $n_n=2$ ,  $n_p=2$ , and  $n_h=0$ ) and  $k=1.0$ . The dotted line is with  $k=2.0$ . The dashed line is with  $n_o=3$  ( $n_n=2$ ,  $n_p=1$ , and  $n_h=0$ ) and  $k=1.0$ , normalized to experimental values at the maximum cross-section point with normalization constant  $N=0.93$  for all the curves.

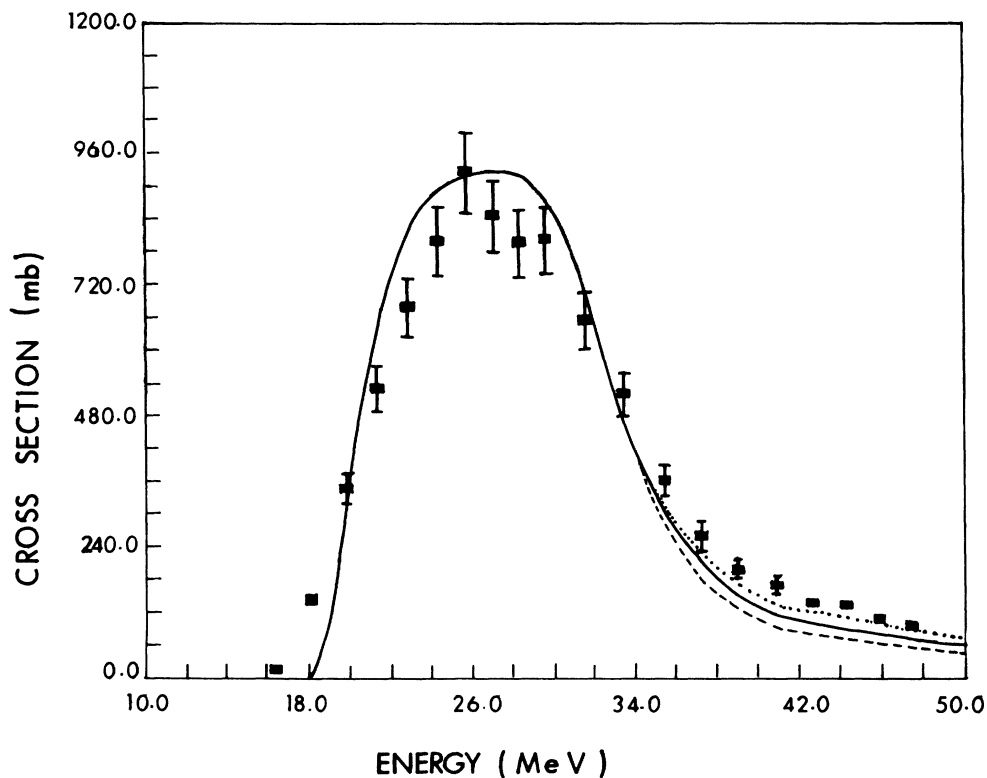


FIG. 5. The total residual production cross section in mb for the reaction  $^{69}\text{Ga}(\alpha, 2n)^{71}\text{As}$  (■ symbols) is plotted as a function of  $\alpha$ -particle bombarding energy. Dashed line is the hybrid model calculation with  $n_o=4$  ( $n_n=2$ ,  $n_p=2$ , and  $n_h=0$ );  $k=1.0$  and  $N=1.119$ , solid line is with  $k=1.5$  and  $N=1.127$  and dotted line with  $k=2.0$  and  $N=1.134$ .

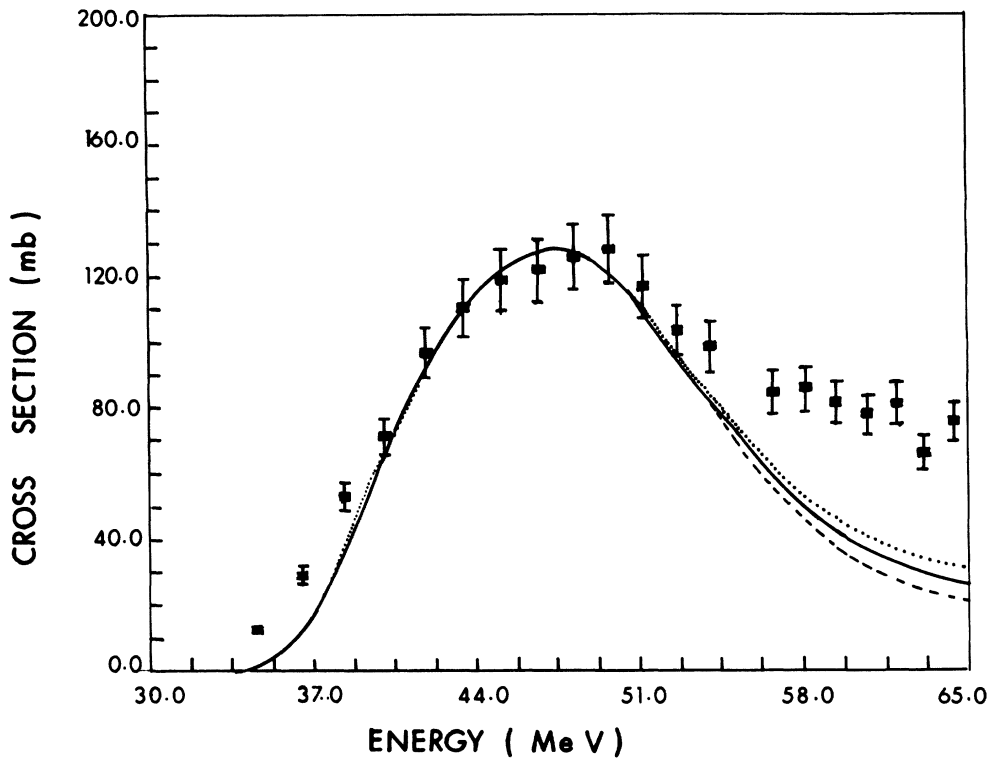


FIG. 6. The total residual production cross section in mb for the reaction  $^{69}\text{Ga}(\alpha, 2p4n)^{67}\text{Ga}$  (■ symbols) is plotted as a function of  $\alpha$ -particle bombarding energy. Dashed line is the hybrid model calculation with  $n_o=4$  ( $n_n=2$ ,  $n_p=2$ , and  $n_h=0$ );  $k=1.0$  and  $N=0.383$ , solid line is with  $k=1.5$  and  $N=0.427$  and dotted line with  $k=2.0$  and  $N=0.468$ .

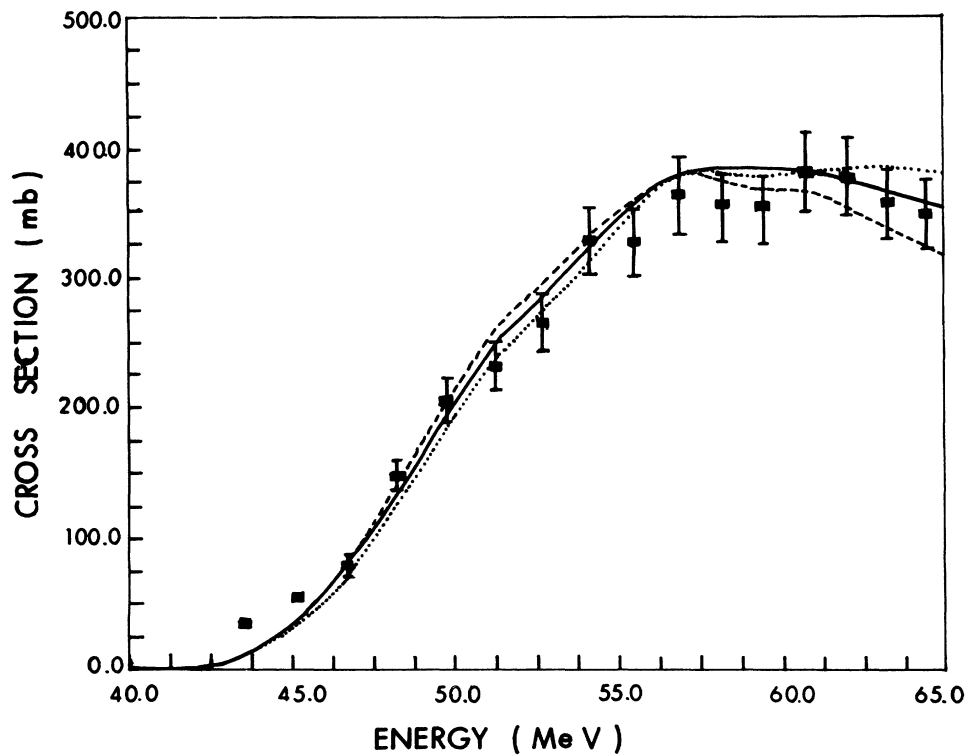


FIG. 7. The total residual production cross section in mb for the reaction  $^{69}\text{Ga}(\alpha, p3n)^{69}\text{Ge}$  (■ symbols) is plotted as a function of  $\alpha$ -particle bombarding energy. Dashed line is the hybrid model calculation with  $n_o=4$  ( $n_n=2$ ,  $n_p=2$ , and  $n_h=0$ );  $k=1.0$  and  $N=0.755$ , solid line is with  $k=1.5$  and  $N=0.798$  and dotted line with  $k=2.0$  and  $N=0.833$ .

**C. Integral excitation function  
for  $\alpha$ -induced reaction on  $^{71}\text{Ga}$**

In Table IV and Figs. 8–10 our experimental results for the production of  $^{71}\text{As}$ ,  $^{72}\text{As}$ , and  $^{74}\text{As}$  radionuclides via  $\alpha$ -induced reactions on  $^{71}\text{Ga}$  are summarized. The uncertainty in energy values includes those of target thickness and beam energy resolution ( $\pm 0.2$  MeV) only as mentioned in Sec. III A. The cross sections are in millibarns and uncertainties are  $\leq 8\%$ .

**D. Integral excitation function  
for  $\alpha$ -induced reaction on  $^{121}\text{Sb}$**

In Table V and Figs. 11–14 our experimental results for the production of  $^{124}\text{I}$ ,  $^{123}\text{I}$ ,  $^{121}\text{I}$ , and  $^{121}\text{Te}$  radionuclides via  $\alpha$ -induced reactions on  $^{121}\text{Sb}$  are summarized. The uncertainty given for the energy values includes

those of target thickness and beam energy resolution ( $\pm 0.2$  MeV) only. Since the radionuclides  $^{124}\text{I}$  and  $^{123}\text{I}$  could also be produced via  $(\alpha, 3n)$  and  $(\alpha, 4n)$  reactions on  $^{123}\text{Sb}$ , respectively, in the overlapping region these cross sections are taken as proportional to their theoretical values based on the hybrid model of Blann.<sup>24</sup> These points are marked with symbol (\*) in Tables V and VI. The cross sections are in millibarns and the uncertainties are  $< 8\%$ . Only a few experimental data on  $\alpha$ -induced reactions on  $^{121}\text{Sb}$  exist in the literature. In 1982 A. Colboreanu *et al.*<sup>25</sup> measured the  $^{121}\text{Sb}(\alpha, n)^{124}\text{I}$  and  $^{121}\text{Sb}(\alpha, 2n)^{123}\text{I}$  cross sections in the energy range 11.5–27.0 MeV. For the  $^{121}\text{Sb}(\alpha, 2n)^{123}\text{I}$  reaction the agreement between the present work and their measurement is reasonably good in the overlapping region as shown in Fig. 15, but for the  $(\alpha, n)$  reaction (not shown) the difference is appreciable. Since no data exist in the literature for  $\alpha$ -induced reactions on  $^{123}\text{Sb}$ , therefore, no comparison could be made with other measurements.

TABLE IV. Experimental cross section for the  $\alpha$ -induced reaction on  $^{71}\text{Ga}$ .

$E_\alpha$ (MeV)	$^{71}\text{Ga}(\alpha, n)^{64}\text{As}$ (mb)	$^{71}\text{Ga}(\alpha, 3n)^{72}\text{As}$ (mb)	$^{71}\text{Ga}(\alpha, 4n)^{71}\text{As}$ (mb)
10.10±0.25	56.8±4.5		
12.36±0.25	435.5±34.8		
14.42±0.25	722.7±57.8		
16.33±0.25	559.1±44.7		
18.06±0.24	365.5±29.2		
19.76±0.24	190.1±15.2		
21.33±0.12	111.2±8.9		
22.85±0.11	72.4±5.8		
24.28±0.23	58.9±4.7		
25.68±0.23	60.5±4.8		
27.01±0.23	42.9±3.4		
28.14±0.22		195.7±15.6 *	
30.36±0.22		408.2±32.6 *	
32.54±0.22		570.8±38.9	
34.54±0.22		721.±54.3	
36.40±0.22		837.1±67.5	
38.31±0.21		882.6±69.9	
40.09±0.21		942.2±75.1	
41.82±0.21		975.4±78.0	177.8±14.0 *
43.50±0.21		819.2±65.9	280.0±22.0 *
45.13±0.21		767.5±60.1	305.3±25.1
46.71±0.21		684.3±52.9	318.1±26.4
48.25±0.21		620.2±49.8	381.6±31.5
49.76±0.21		534.8±47.1	457.2±37.4
51.23±0.21		441.9±36.1	427.1±34.6
52.67±0.21		393.8±32.1	423.7±32.7
54.08±0.21		347.7±27.6	457.0±37.0
55.46±0.21		298.6±25.0	406.0±32.4
56.81±0.21		273.5±22.4	413.9±32.1
58.14±0.21		235.8±17.5	407.2±32.3
59.44±0.21		228.6±18.1	376.7±29.1
60.71±0.20		208.4±15.2	378.2±35.5
61.96±0.20		208.9±16.1	378.2±30.2
63.20±0.20		186.1±14.2	353.5±29.5
64.42±0.20		184.6±14.1	353.2±28.6

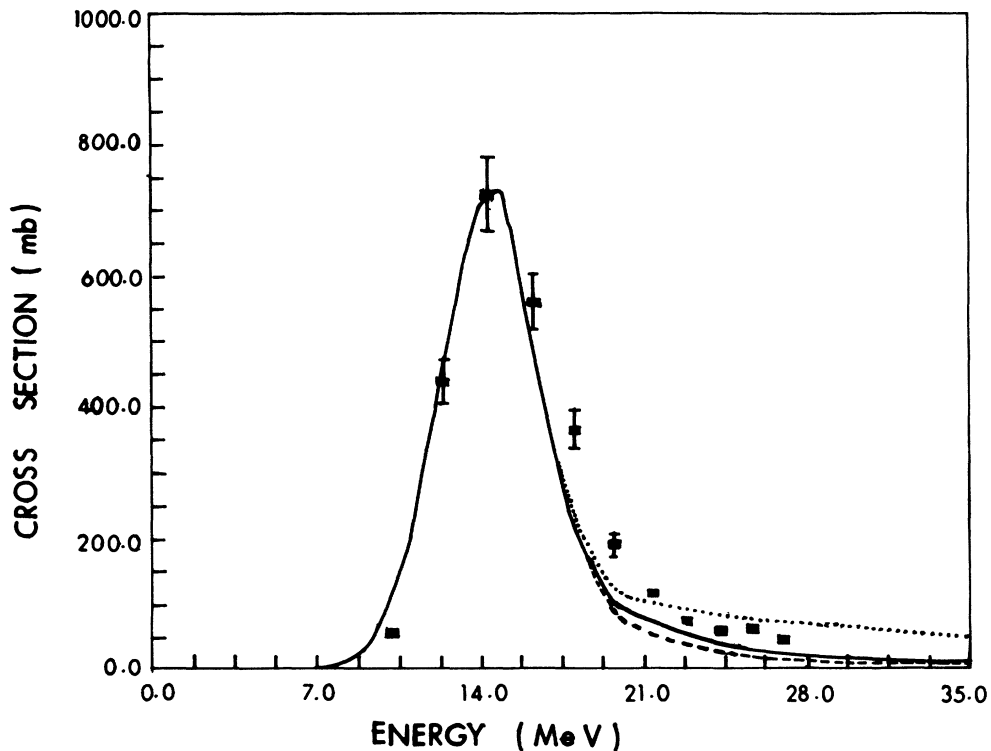


FIG. 8. The total residual production cross section in mb for the reaction  $^{71}\text{Ga}(\alpha, n)^{74}\text{As}$  (■ symbols) is plotted as a function of  $\alpha$ -particle bombarding energy. Dashed line is the hybrid model calculation with  $n_o = 4$  ( $n_n = 2$ ,  $n_p = 2$ , and  $n_h = 0$ );  $k = 1.0$  and  $N = 1.05$ , solid line is with  $k = 2.0$  and  $N = 1.05$  and dotted line is with  $n_o = 3$  ( $n_n = 2$ ,  $n_p = 1$ , and  $n_h = 0$ );  $k = 1.0$  and  $n = 1.05$ .

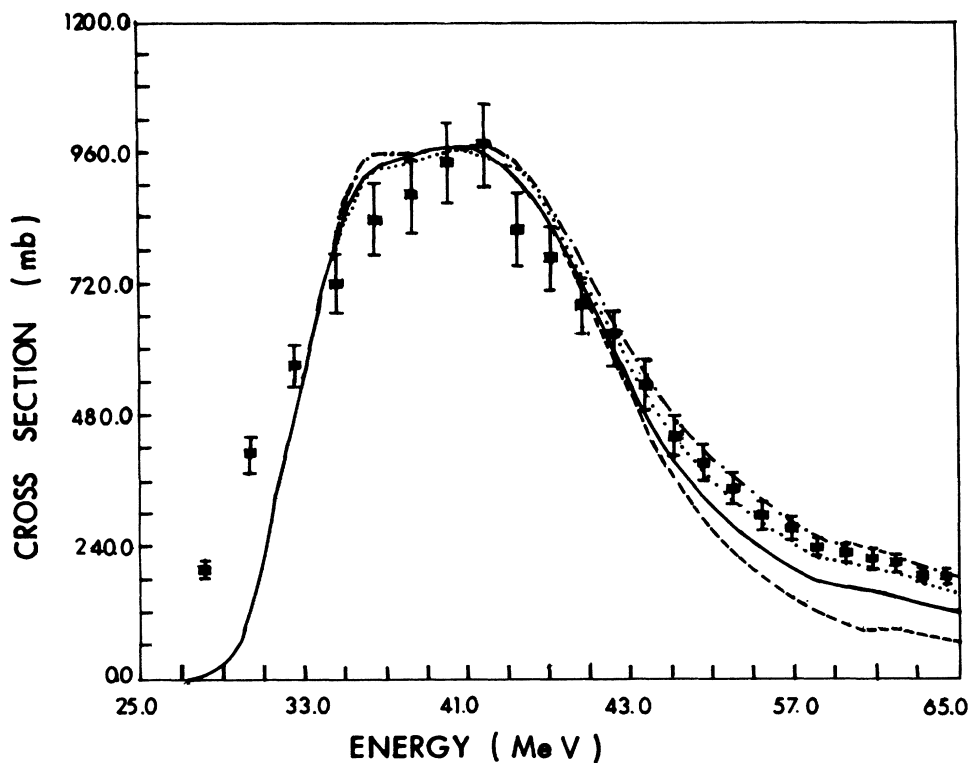


FIG. 9. The total residual production cross section in mb for the reaction  $^{71}\text{Ga}(\alpha, 3n)^{72}\text{As}$  (■ symbols) is plotted as a function of  $\alpha$ -particle bombarding energy. Dashed line is the hybrid model calculation with  $n_o = 6$  ( $n_n = 4$ ,  $n_p = 2$ , and  $n_h = 0$ );  $k = 1.0$  and  $N = 1.017$ , solid line is the hybrid model calculation with  $n_o = 4$  ( $n_n = 2$ ,  $n_p = 2$ , and  $n_h = 0$ );  $k = 1.0$  and  $N = 1.071$ , dotted line is with  $k = 1.5$  and  $N = 1.128$  and dot-dashed line with  $k = 2.0$  and  $N = 1.159$ .

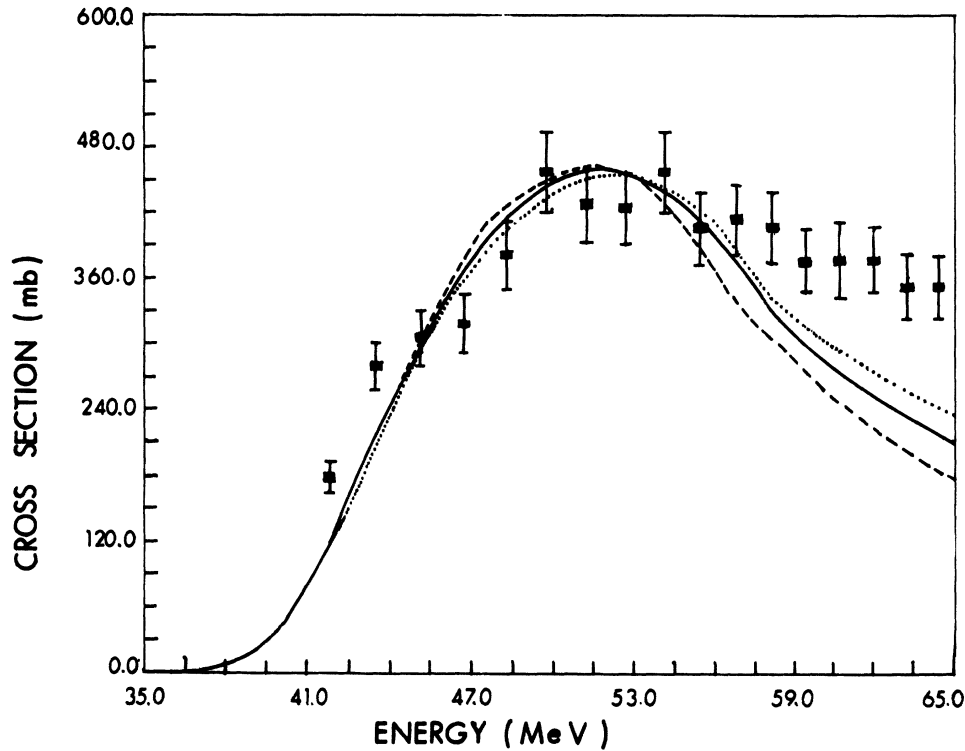


FIG. 10. The total residual production cross section in mb for the reaction  $^{71}\text{Ga}(\alpha,4n)^{72}\text{As}$  (■ symbols) is plotted as a function of  $\alpha$ -particle bombarding energy. Dashed line is the hybrid model calculation with  $n_o=4$  ( $n_n=2$ ,  $n_p=2$ , and  $n_h=0$ );  $k=1.0$  and  $N=1.25$ , solid line is with  $k=1.5$  and  $N=1.353$  and dotted line with  $k=2.0$  and  $N=1.430$ .

TABLE V. Experimental cross section for the  $\alpha$ -induced reaction on  $^{121}\text{Sb}$ .

$E$ (MeV)	$^{121}\text{Sb}(\alpha,n)^{124}\text{I}$ (mb)	$^{121}\text{Sb}(\alpha,2n)^{123}\text{I}$ (mb)	$^{121}\text{Sb}(\alpha 4n)^{121}\text{I}$ (mb)	$^{121}\text{Sb}(\alpha,p3n)^{121}\text{Te}$ (mb)
57.32±0.20			666.56±53.33	494.97±39.58
55.91±0.20			932.62±74.6	702.92±56.23
54.50±0.20			1388.93±111.1	1005.17±80.42
53.10±0.20			1574.74±125.98	1135.00±90.80
51.65±0.20			1579.14±126.33	1131.82±90.54
50.20±0.20			1575.48±125.96	1076.13±86.09
48.70±0.20			1523.32±121.9	989.10±79.13
47.20±0.20			1229.76±98.4	855.61±68.45
45.60±0.20			1155.53±92.4	725.33±58.02
44.15±0.20		141.07±11.29 *		
44.01±0.27			665.50±53.24	449.66±35.98
42.42±0.21		166.26±13.30 *		
42.28±0.20			497.82±82.0	318.85±25.51
40.60±0.33		180.44±14.44 *	209.24±16.74	134.78±10.78
38.70±0.20		239.46±18.45 *	64.62±5.17	45.88±3.67
36.70±0.25		361.18±28.89	10.51±0.84	
34.40±0.30		514.01±41.12		
33.24±0.30		687.18±54.97		
31.80±0.24		924.22±73.94		
30.50±0.21	4.31±0.34 *	897.63±71.33		
29.00±0.26	8.20±0.66 *	1265.74±101.26		
27.51±0.30	9.94±0.80 *	1389.27±111.14		
25.90±0.35	20.35±1.63 *	1213.94±97.11		
24.20±0.27	64.77±5.18	1145.44±91.64		
22.50±0.31	115.79±9.26	1010.39±80.83		
20.58±0.35	210.39±16.83	733.24±58.66		
18.50±0.41	352.73±28.16	371.62±29.73		
16.40±0.28	309.99±24.72	40.26±3.22		
14.10±0.47	99.23±7.94	1.46±0.11		

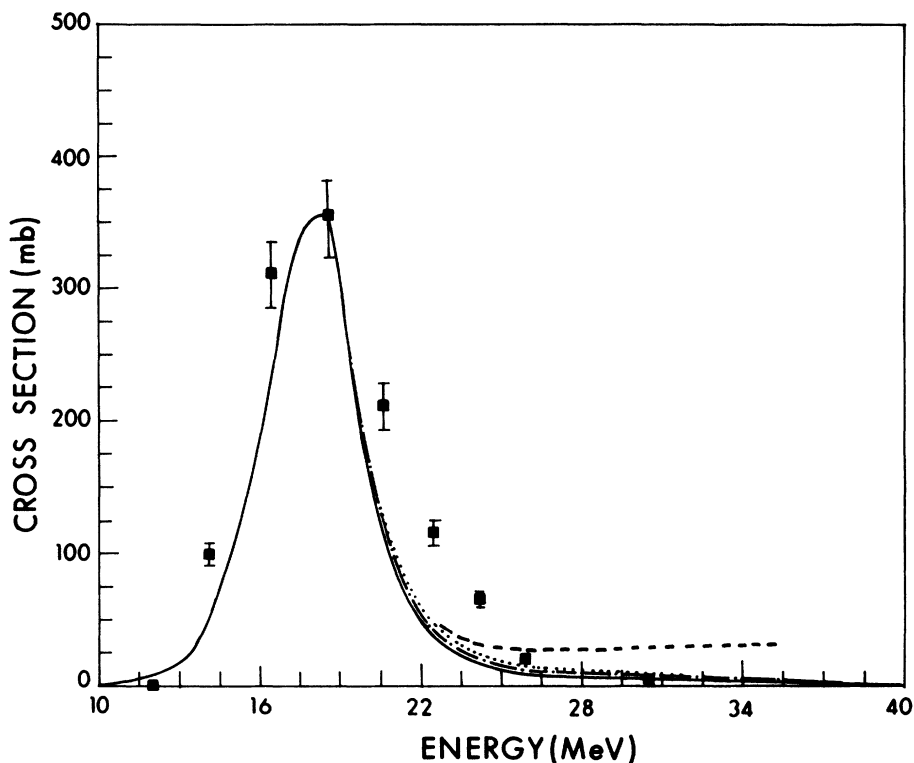


FIG. 11. The total residual production cross section in mb for the reaction  $^{121}\text{Sb}(\alpha, n)^{124}\text{I}$  (■ symbols) is plotted as a function of  $\alpha$ -particle bombarding energy. Solid line is the hybrid model calculation with  $n_o = 4$  ( $n_n = 2$ ,  $n_p = 2$ , and  $n_h = 0$ );  $k = 1.0$ , dot-dashed line with  $k = 1.5$ , and dotted line with  $k = 2.0$ . The dashed line is with  $n_o = 3$  ( $n_n = 2$ ,  $n_p = 1$ , and  $n_h = 0$ ) and  $k = 1.0$ , normalized to experimental values at the maximum cross-section point with normalization constant  $N = 0.71$  for all the curves.

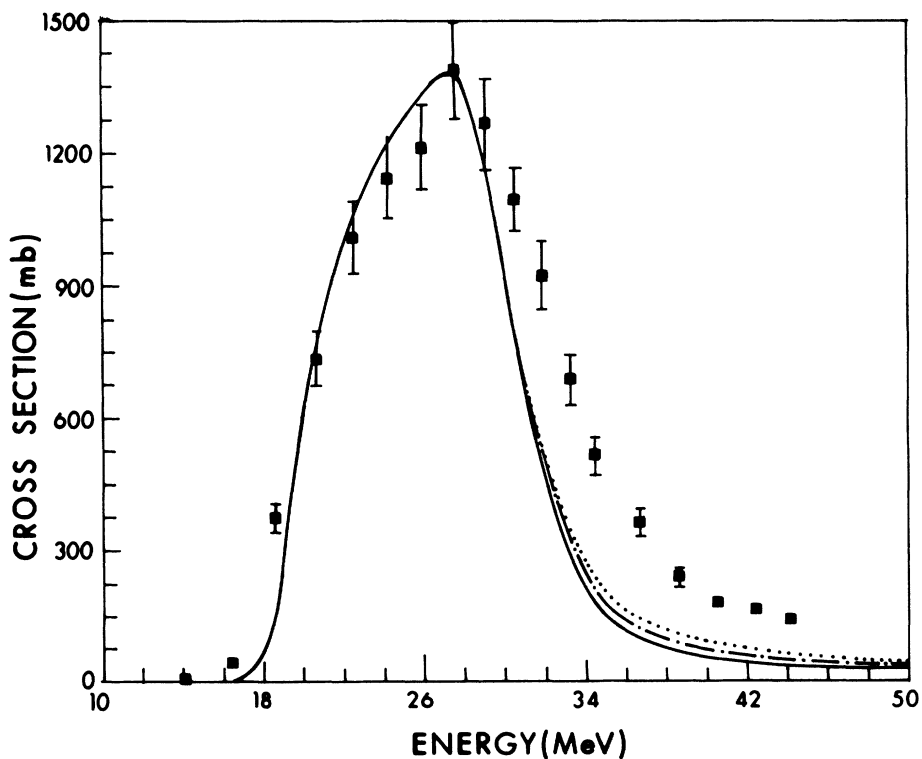


FIG. 12. The total residual production cross section in mb for the reaction  $^{121}\text{Sb}(\alpha, 2n)^{123}\text{I}$  (■ symbols) is plotted as a function of  $\alpha$ -particle bombarding energy. Solid line is the hybrid model calculation with  $n_o = 4$  ( $n_n = 2$ ,  $n_p = 2$ , and  $n_h = 0$ );  $k = 1.0$  and  $N = 1.114$  solid line is with  $k = 1.5$  and  $N = 1.120$  and dotted line with  $k = 2.0$  and  $N = 1.126$ .

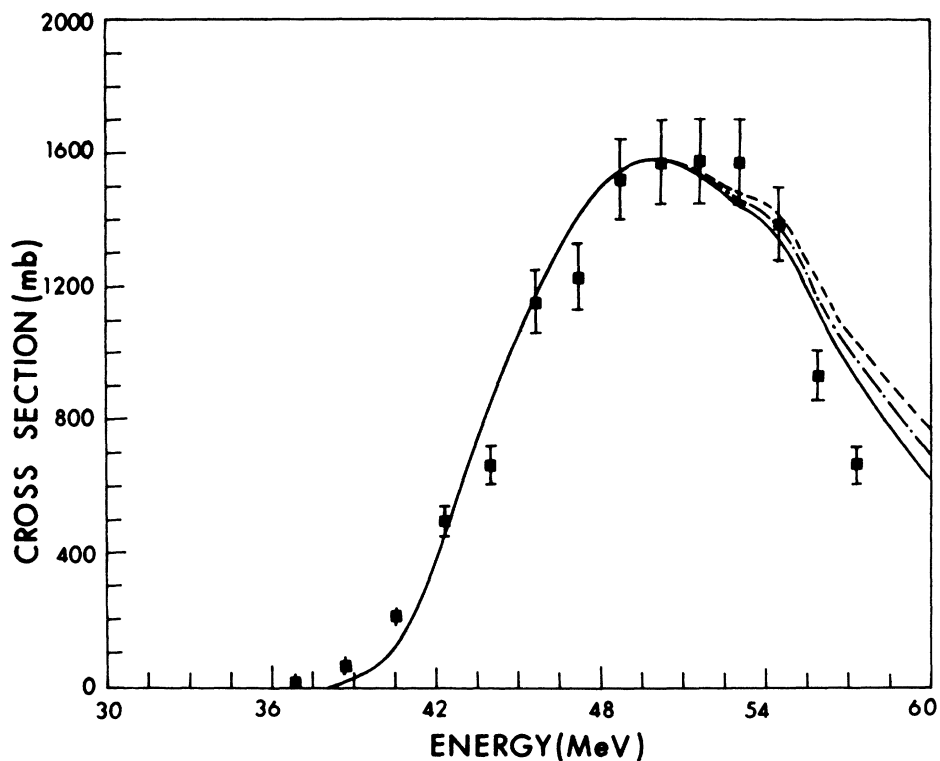


FIG. 13. The total residual production cross section in mb for the reaction  $^{121}\text{Sb}(\alpha,4n)^{121}\text{I}$  (■ symbols) is plotted as a function of  $\alpha$ -particle bombarding energy. Solid line is the hybrid model calculation with  $n_o=4$  ( $n_n=2$ ,  $n_p=2$ , and  $n_h=0$ );  $k=1.0$  and  $N=1.523$ , solid line is with  $k=1.5$  and  $N=1.628$  and dotted line with  $k=2.0$  and  $N=1.728$ .

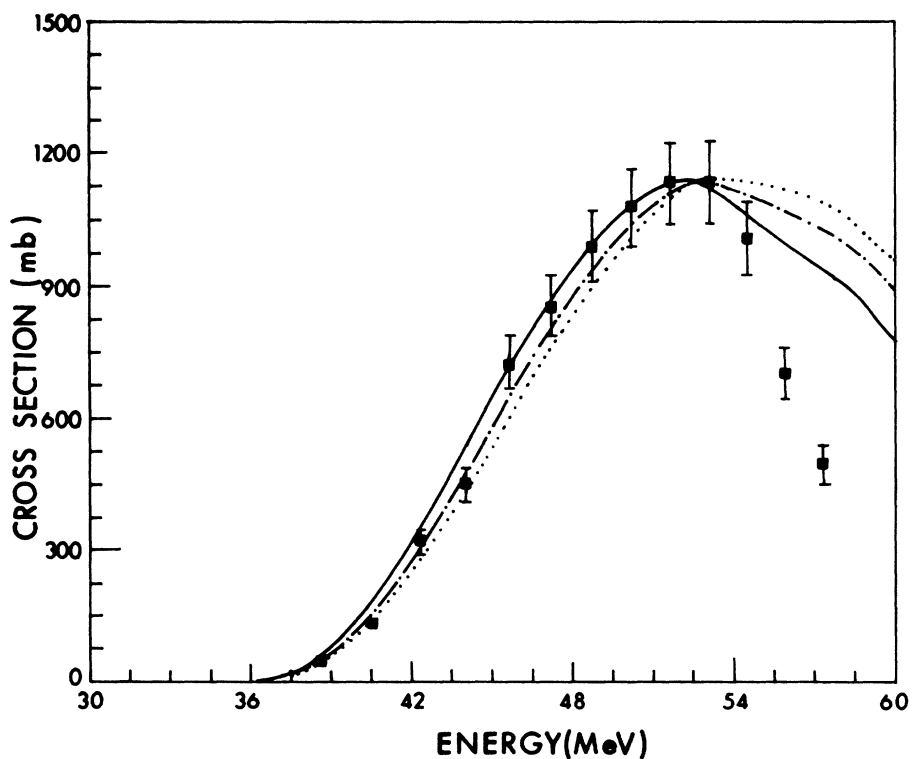


FIG. 14. The total residual production cross section in mb for the reaction  $^{121}\text{Sb}(\alpha,p3n)^{121}\text{Te}$  (■ symbols) is plotted as a function of  $\alpha$ -particle bombarding energy. Solid line is the hybrid model calculation with  $n_o=4$  ( $n_n=2$ ,  $n_p=2$ , and  $n_h=0$ );  $k=1.0$  and  $N=3.920$ , solid line is with  $k=1.5$  and  $N=3.640$  and dotted line with  $k=2.0$  and  $N=3.440$ .

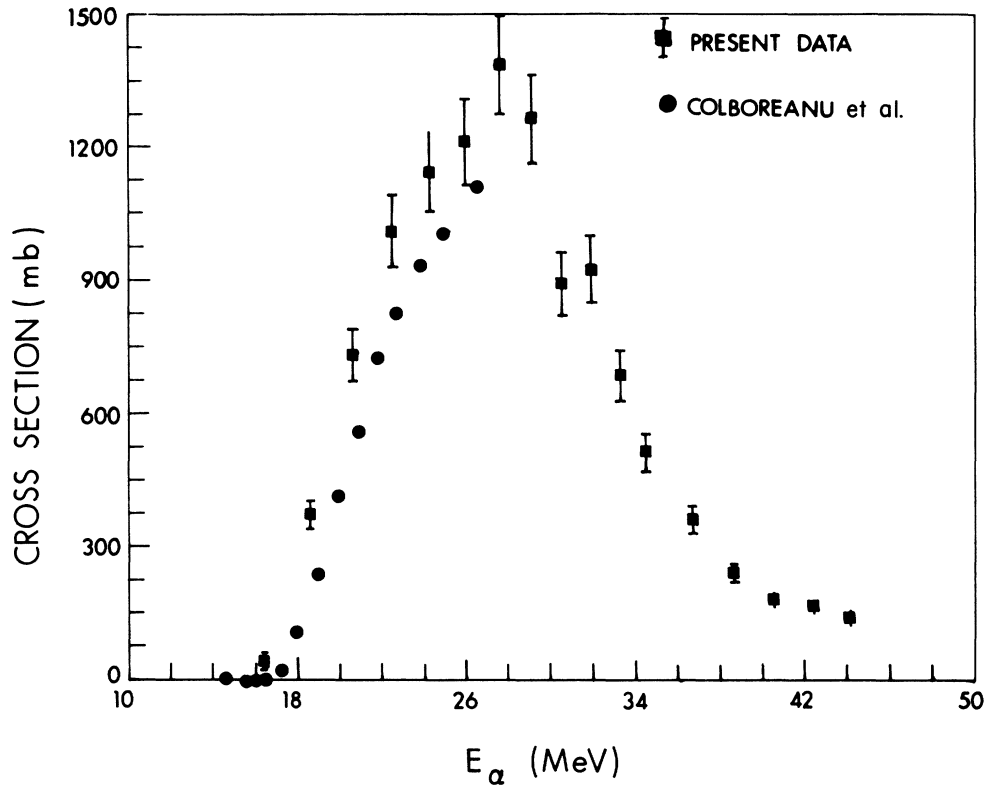


FIG. 15. The total residual production cross section in mb for the reaction  $^{121}\text{Sb}(\alpha, 2n)^{123}\text{I}$  [■ symbols, our measurements; ● symbols, the measurements by Colboreanu *et al.* (Ref. 17)] is plotted as a function of  $\alpha$ -particle bombarding energy.

TABLE VI. Experimental cross section for the  $\alpha$ -induced reaction on  $^{123}\text{Sb}$ .

$E_\alpha$ (MeV)	$^{123}\text{Sb}(\alpha, n)^{126}\text{I}$ (mb)	$^{123}\text{Sb}(\alpha, 3n)^{124}\text{I}$ (mb)	$^{123}\text{Sb}(\alpha, 4n)^{123}\text{I}$ (mb)
57.32±0.20		65.12±5.18	475.51±38.04
55.91±0.20		91.40±7.28	710.38±56.83
54.50±0.20		131.71±10.49	1101.70±88.14
53.10±0.20		130.63±10.40	1315.49±105.24
51.65±0.20		160.87±12.80	1401.70±112.14
50.20±0.02		195.55±15.57	1484.12±118.73
48.70±0.20		255.79±20.40	1510.37±120.83
47.20±0.20		315.75±25.12	1414.55±113.16
45.60±0.20		520.04±41.36	1409.75±112.78
44.15±0.20		703.36±56.08	
44.01±0.27			1053.46±84.28
42.28±0.20		820.03±65.28	967.55±77.40
40.60±0.33		949.86±75.99	675.26±54.02
38.70±0.20		1131.53±90.08	353.68±28.29 *
36.70±0.25		1299.02±103.44	83.84±6.70 *
34.40±0.30		1199.63±95.59	2.58±0.21 *
33.21±0.30		1088.50±86.80	
31.80±0.24		911.88±72.72	
30.50±0.21		659.90±52.64 *	
29.00±0.26	23.23±1.86	448.88±35.84 *	
27.51±0.30	26.06±2.08	221.24±17.65 *	
27.51±0.30	27.38±2.19		
25.90±0.35	38.54±3.08	48.07±3.84 *	
24.20±0.27	56.15±4.49		
22.50±0.31	83.87±6.71		
20.58±0.35	142.97±11.44		
18.50±0.41	216.61±17.33		
16.40±0.28	160.36±12.83		
14.10±0.47	11.69±0.94		

### E. Integral excitation function for $\alpha$ -induced reaction on $^{123}\text{Sb}$

In Table VI and Figs. 16–18 our experimental results for the production of  $^{126}\text{I}$ ,  $^{124}\text{I}$ , and  $^{123}\text{I}$  radionuclides via  $\alpha$ -induced reactions on  $^{123}\text{Sb}$  are summarized. The uncertainty in energy values includes those of target thickness and beam energy resolution ( $\pm 0.2$  MeV) only as mentioned in Sec. III A. The cross sections are in millibarns and uncertainties are  $\leq 8\%$ . Since no data exists in the literature for  $\alpha$ -induced reactions on  $^{123}\text{Sb}$ , therefore, no comparison could be made with other measurements.

### F. Cross-section for $\alpha$ -induced reaction on $^{27}\text{Al}$

Since the reaction  $^{27}\text{Al}(\alpha, 4p 3n)^{24}\text{Na}$  and  $^{27}\text{Al}(\alpha, 4p 5n)^{22}\text{Na}$  had been studied extensively in the past,<sup>18,26</sup> we have checked the quality of our absolute cross-section values by measuring the cross section for these reactions by way of target backing and energy degrader foils in the stacks. A comparison of the production cross sections for  $^{24}\text{Na}$  and  $^{22}\text{Na}$  with other authors<sup>18,26</sup> shows the agreement with other work is reasonably good. Our measurements are summarized in Table VII and Fig. 19. The threshold of the above-mentioned

reactions without cluster emission is very high (see Table I); therefore, the nuclides  $^{22}\text{Na}$  and  $^{24}\text{Na}$  are produced only by cluster emission in the energy range over which present measurements have been made. The Alice code of Blann<sup>24</sup> does not consider cluster emission for hybrid model calculation; no theoretical calculation was, therefore, done for these two reactions.

## IV. COMPARISON WITH THEORETICAL PREDICTIONS

A rigorous theory of nuclear reaction for which calculations can be performed to describe mass, angular and energy distribution data from intermediate energy collisions with complex particles is presently not available. A simpler compound-nucleus model<sup>27</sup> is clearly not applicable above 10 MeV/nucleon owing to large probability for preequilibrium processes. In the preequilibrium models, on the other hand, it is difficult to extract kinematic information.<sup>12</sup> An alternative approach is to the intranuclear cascade model,<sup>13</sup> which has been extended to  $\alpha$ -induced reaction.<sup>13</sup> In considering the interaction of an energetic projectile with a complex nucleus, Serber<sup>15</sup> originally separated the reaction into two stages. In the first

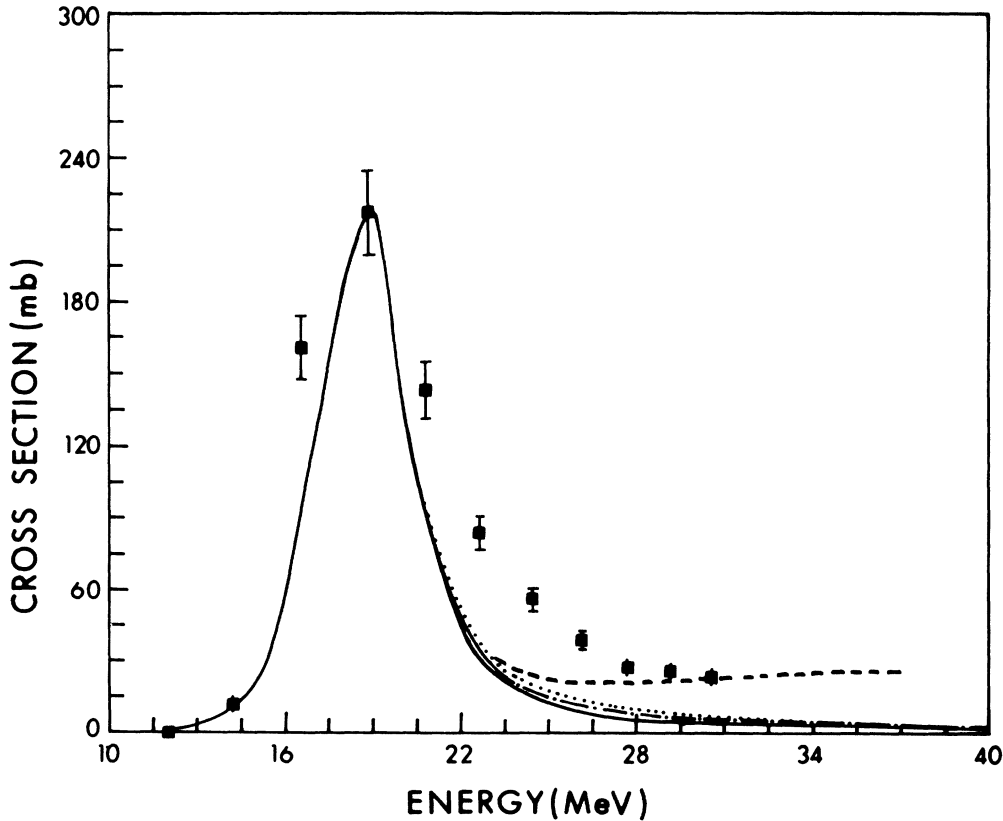


FIG. 16. The total residual production cross section in mb for the reaction  $^{123}\text{Sb}(\alpha, n)^{126}\text{I}$  (■ symbols) is plotted as a function of  $\alpha$ -particle bombarding energy. Solid line is the hybrid model calculation with  $n_o = 4$  ( $n_n = 2$ ,  $n_p = 2$ , and  $n_h = 0$ );  $k = 1.0$ , dot-dashed line with  $k = 1.5$ , and dotted line with  $k = 2.0$ . The dashed line is with  $n_o = 3$  ( $n_n = 2$ ,  $n_p = 1$ , and  $n_h = 0$ ) and  $k = 1.0$ , normalized to experimental values at the maximum cross-section point with normalization constant  $N = 0.54$  for all the curves.

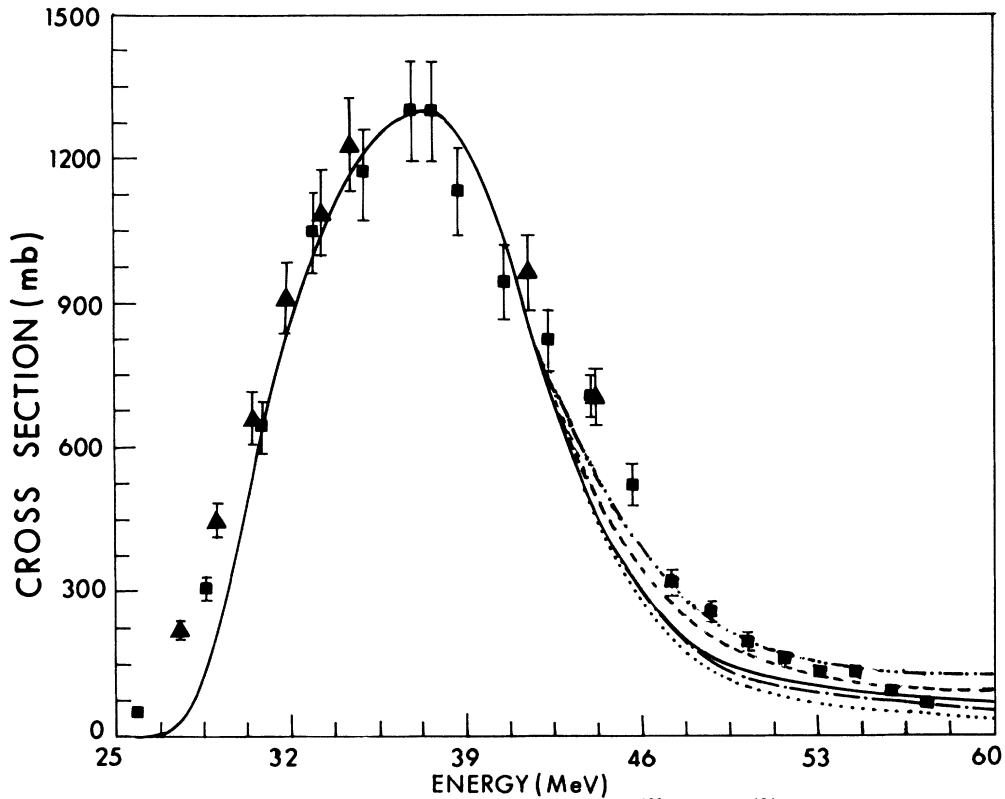


FIG. 17. The total residual production cross section in mb for the reaction  $^{123}\text{Sb}(\alpha, 3n)^{124}\text{I}$  (■ symbols) is plotted as a function of  $\alpha$ -particle bombarding energy. The dotted line is the hybrid model calculation with  $n_0=6$  ( $n_n=4$ ,  $n_p=2$ , and  $n_h=0$ );  $k=1.0$  and  $N=0.856$ , the dot-dashed line is the hybrid model calculation with  $n_0=5$  ( $n_n=3$ ,  $n_p=2$ , and  $n_h=0$ );  $k=1.0$  and  $N=0.868$  and solid line is the hybrid model calculation with  $n_0=4$  ( $n_n=2$ ,  $n_p=2$ , and  $n_h=0$ );  $k=1.0$  and  $N=0.885$ , dashed line is with  $k=1.5$  and  $N=0.906$  and double dot-dashed line with  $k=2.0$  and  $N=0.925$ .

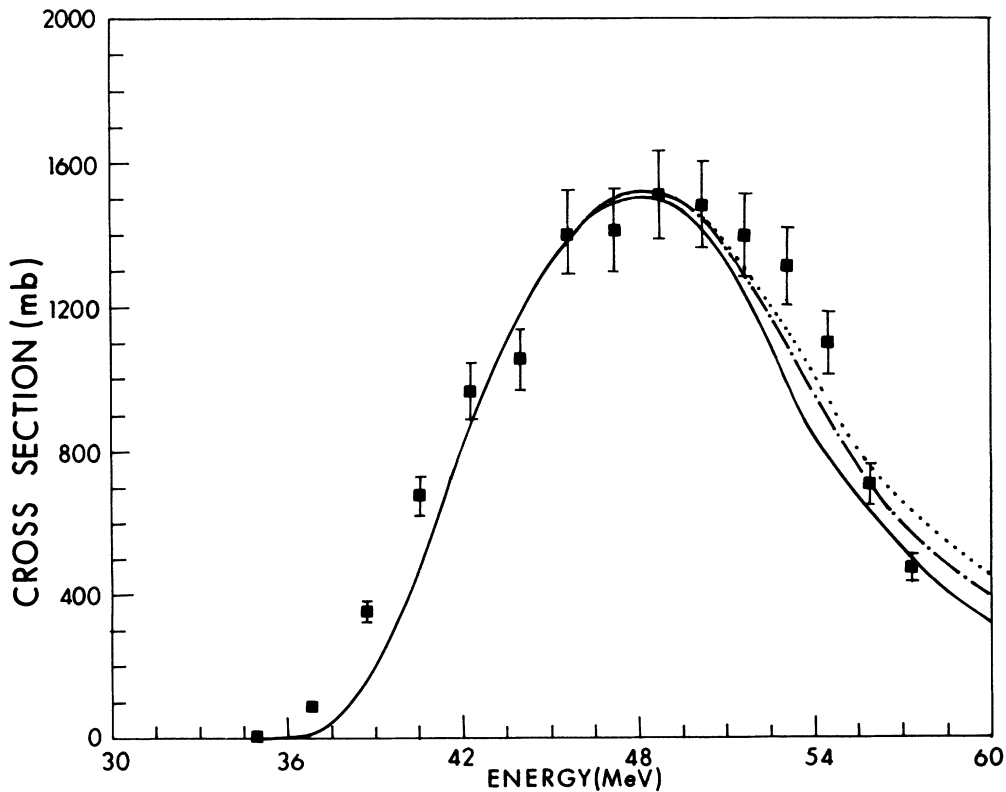


FIG. 18. The total residual production cross section in mb for the reaction  $^{123}\text{Sb}(\alpha, 4n)^{123}\text{I}$  (■ symbols) is plotted as a function of  $\alpha$ -particle bombarding energy. Solid line is the hybrid model calculation with  $n_0=4$  ( $n_n=2$ ,  $n_p=2$ , and  $n_h=0$ );  $k=1.0$  and  $N=1.130$ , solid line is with  $k=1.5$  and  $N=1.210$  and dotted line with  $k=2.0$  and  $N=1.270$ .

TABLE VII. Experimental cross section for the  $\alpha$ -induced reaction on Al.

$E_\alpha$ (MeV)	$^{127}\text{Al}(\alpha, 4p3n)^{24}\text{Na}$ (mb)	$^{27}\text{Al}(\alpha, 4p5n)^{22}\text{Na}$ (mb)
32.54±2.00	0.24±0.02	
34.54±1.92	0.27±0.02	
36.46±1.84	0.30±0.02	
38.31±1.78	0.36±0.03	4.1±0.3
40.09±1.71	0.51±0.04	4.1±0.3
41.82±1.66	0.75±0.06	9.1±0.7
43.50±1.61	1.06±0.09	15.1±1.2
45.13±1.56	1.48±0.12	20.1±1.6
46.71±1.52	2.07±0.17	26.4±2.1
48.25±1.48	2.93±0.23	33.1±2.6
49.76±1.45	4.05±0.32	41.8±3.3
51.23±1.41	5.40±0.43	42.8±3.4
52.67±1.38	7.19±0.58	46.1±3.7
54.08±1.35	9.09±0.73	44.7±3.6
55.46±1.33	12.33±0.99	39.3±3.1
56.81±1.30	14.81±1.18	37.5±3.0
57.81±0.65	18.29±1.46	
58.14±1.28	20.28±1.62	36.3±2.9
59.11±0.64	20.92±1.67	
59.44±1.25	23.76±1.90	37.3±3.0
60.41±0.63	24.47±1.96	
60.71±1.23	27.10±2.16	33.8±2.7
61.66±0.61	27.10±2.17	
61.96±1.21	29.62±2.37	31.24±2.5
62.90±0.60	29.73±2.38	
63.20±1.20	33.00±2.64	28.6±2.3
64.12±0.59	32.19±2.58	
64.42±1.18	32.73±2.61	26.1±2.1

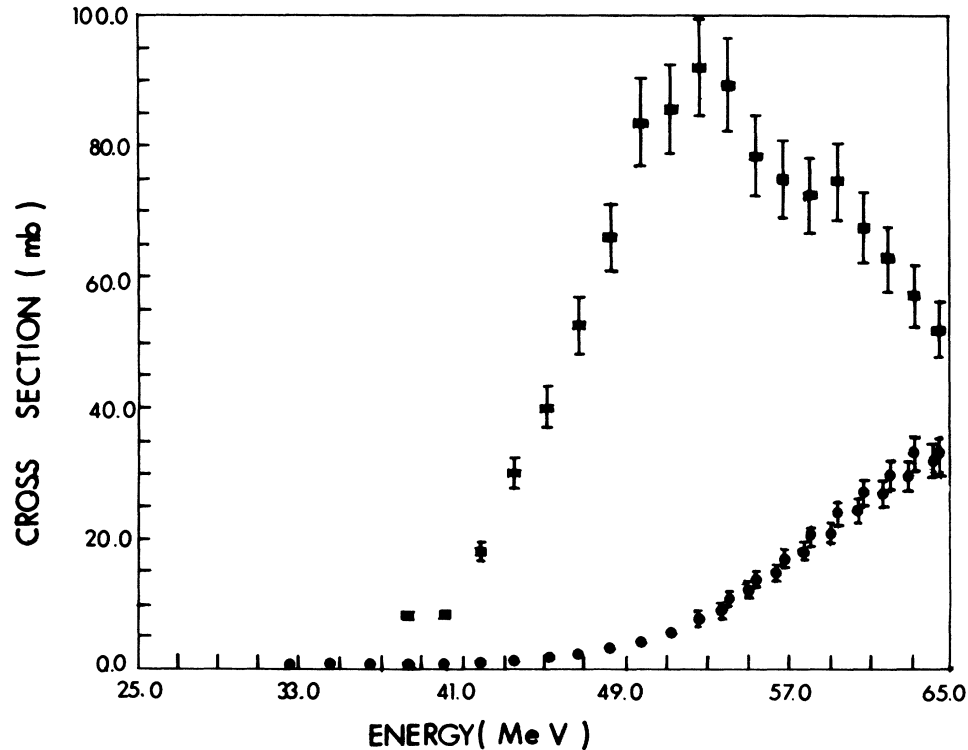


FIG. 19. The total residual production cross section in mb for the reaction  $^{27}\text{Al}(\alpha, 4p5n)^{22}\text{Na}$  (■ symbols) after having been multiplied by a factor of 2 and  $^{27}\text{Al}(\alpha, 4p3n)^{24}\text{Na}$  (● symbols) are plotted as a function of  $\alpha$ -particle bombarding energy.

stage, the incident particle initiates a nucleon-nucleon cascade in the target nucleus on a time scale comparable to nuclear transit times. Cascade nucleons, which acquire sufficient energy, then escape from the target, leaving an excited residual nucleus. The second stage involves equilibration of the energy deposited in the residual nucleus and the subsequent statistical deexcitation process, which occurs on a much longer time scale. Usually a nuclear evaporation process is utilized to describe this process.<sup>16,17</sup> Nuclear reaction models to treat the preequilibrium phase of reactions leading to the formation of a compound nucleus have been around for many years.<sup>1-6,13,28-30</sup> Most of these models are semiclassical in nature and have been used with considerable success in describing experimental data pertaining to the equilibration process, mainly the forward peaked hard component observed in the continuous spectra of light ejectiles and the high-energy tails seen in the excitation functions of activation cross sections. However, most of these models employ one or both of the two basic concepts: the intranuclear cascade model (INC) of Goldberger<sup>13</sup> as mentioned before and Griffin's statistical model of intermediate structure (SMI's).<sup>3</sup> The idea in the INC approach is to treat equilibration as a series of quasifree scattering processes of independent nucleons in the nuclear environment and to follow these processes explicitly in a geometric fashion. Nucleon-nucleon kinematics and cross section are employed and emission is assumed to occur whenever a nucleon follows a trajectory out of the composite nucleus without undergoing another collision. Griffin's idea, on the other hand, was to consider the equilibration system as a whole, envisioning it to pass through increasingly complex configurations of single-particle excitation. It goes on to assume that, at each stage, all possible configurations are equally likely so that the occurrence of configurations capable of particle emission into continuum may be estimated on a statistical basis. However, the SMIS does not explicitly treat the competition between particle emission and intranuclear transition and therefore cannot predict absolute cross sections. The integral excitation functions of  $\alpha$ -induced reactions have been discussed by several authors<sup>1-6,11-17</sup> considering models of the compound nucleus as well as of preequilibrium reactions, as mentioned above. They conclude that the theory of preequilibrium reactions is helpful in explaining the mechanism of  $\alpha$ -induced reactions. In the present work our excitation functions are calculated on the basis of hybrid model<sup>1</sup> using the program Overlaid Alice<sup>24</sup> on the IRIS-80 computer at our center. The calculations were done in 2 MeV steps from 10.0 to 65.0 MeV. The hybrid model for the preequilibrium reaction was proposed by Blann<sup>1</sup> which provides in some way a marriage between the simple SMIS model of Griffin<sup>3</sup> and the INC model using the more elaborate master equation approach due to Harp *et al.*<sup>4,5</sup> Since the program and the theories involved have been discussed by several authors,<sup>1-6,24</sup> we briefly summarize in the Appendix the main points of the hybrid model of preequilibrium theory. For details see Ref. 1.

The statistical part of the Overlaid Alice can account for a large variety of reaction types. Besides evaporation

of neutrons and protons,<sup>31</sup> also clusters such as deuteron and  $\alpha$ -particles can be considered. The nuclear masses were calculated from the Mayers and Swiatecki mass formula,<sup>32,33</sup> liquid drop masses with pairing for Ga, and shell corrected masses with pairing for Sb, for obvious reasons. The inverse cross sections were calculated using the optical-model subroutine of Overlaid Alice,<sup>24</sup> where the optical-model parameters were those of Becchetti and Greenlees.<sup>34</sup> There are three main points of discussion when using the hybrid model option of Overlaid Alice:<sup>24</sup> (i) the initial exciton configuration, (ii) the intranuclear transition rate, and (iii) the mean-free-path multiplier parameter. In most of our calculations we have kept the initial exciton configuration as  $n_o=4$ ,  $n_p=2$ ,  $n_n=2$  and changed the mean free multiplier parameter  $k$  from 1.0 to 2.0 in steps of 0.5.

In the *a priori* formulation of the hybrid model, the intranuclear transition rates are calculated either from the imaginary part of the optical model or from the free nucleon-nucleon scattering cross section.<sup>35</sup> The use of optical potential in calculating intranuclear transition rates for preequilibrium decay models offer distinct advantages at least in principle over the nucleon-nucleon scattering approach. Specifically, the parameters of the optical potential have been determined from the results and trends of a large body of experimental data. The mean-free-path values are therefore based on experimental measurements in nuclear matter as opposed to the extrapolation of free scattering cross sections to the nuclear environment. Secondly, the question of possible errors in the nucleon-nucleon scattering approach due to failure to consider recoil momentum effects is avoided by using the optical potential. Becchetti and Greenlees<sup>34</sup> have analyzed a large body of data to find a best set of optical-model parameters for nucleon induced reactions. But for particle energies exceeding 55 MeV the optical-model parameters of Becchetti and Greenlees<sup>34</sup> are no longer applicable and thus at higher energies the calculation of the mean free path for intranuclear transitions are calculated from nucleon-nucleon scattering cross sections.

The mean-free-path multiplier " $k$ ," which is a kind of free parameter, was introduced by Blann<sup>1</sup> to account for the transparency of nuclear matter in the lower-density nucleus periphery. Considerably better agreements at the high-energy portion of the excitation functions are shown in Figs. 4-18 for the results with " $k$ "=2.0 compared to  $k=1.0$  which implies a mean-free-path (mfp) multiplier for nucleon-nucleon scattering which is  $k=2$  times the values given in Ref. 36. There are several reasons as to why mfp values larger than those calculated in Ref. 36 may be reasonable. First, it is thought that the preequilibrium emission results mainly from high-impact parameter, peripheral target projectile interactions. The lower nuclear density in the nuclear surface should result in a larger mfp for scattering. Secondly the calculations of Ref. 36 were based on the free scattering cross section with only the requirement for scattering within the nucleus, that energy be conserved and that no scattering be allowed into levels below the Fermi energy. However, if the nucleus involved in the scattering process has well-behaved quantum states before and after the transition in

question, then the final states must be accessible from the initial states through coupling with the scattering process. Clearly a fraction of the total states at a given energy are accessible within this restriction of angular momentum conservation and this additional restriction should result in longer mfp for nucleons in nuclear matter.

With respect to initial configuration Blann and Mignerey<sup>37</sup> used  $n_0=4$  ( $n_n=2$ ,  $n_p=2$ ,  $n_h=0$ ) to calculate  $^{59}\text{Co}(\alpha,p)$  spectra. Gadioli *et al.*<sup>38</sup> have also discussed this point in detail and recommended the general application of  $n_0=4$ . With respect to our study the excitation function for the reaction  $^{71}\text{Ga}(\alpha,3n)^{72}\text{As}$  and  $^{123}\text{Sb}(\alpha,3n)^{124}\text{I}$  are most appropriate to examine the initial exciton number for  $\alpha$ -induced reactions on Ga and Sb, respectively. In Figs. 9 and 17 the measured excitation functions are compared with hybrid model results for different initial exciton configurations ( $n_0=4, 5$ , and 6) and mfp multiplier parameter  $k$  varied from 1.0 to 2.0 in steps of 0.5 for  $n_0=4$  ( $n_n=2$ ,  $n_p=2$ ,  $n_h=0$ ) configuration only. Evidently, an initial exciton  $n_0=4$  ( $n_n=2$ ,  $n_p=2$ ,  $n_h=0$ ) configuration which is equivalent to a breakup of the incoming  $\alpha$  particle in the field of the nucleus and the nucleons occupying excited states above the Fermi energy gives a better description of the excitation function compared to other configurations for the  $\alpha$ -particle bombarding energies up to 65.0 MeV. Therefore, we have used mostly  $n_0=4$  ( $n_n=2$ ,  $n_p=2$ ,  $n_h=0$ ) configuration in most of our calculations and varied mfp multiplying parameter  $k$  (which accounts for the transparency of nuclear matter in the lower-density nuclear periphery and angular momentum conservation for nucleon-nucleon scattering in nuclear matter) to fit the excitation function curves.

Figures 4–7 show the fit for  $\alpha$ -induced reaction on  $^{69}\text{Ga}$ , Figs. 8–10 show the fit for  $\alpha$ -induced reaction on  $^{71}\text{Ga}$ , Figs. 11–14 show the fit for  $\alpha$ -induced reaction on  $^{121}\text{Sb}$ , and Figs. 16–18 show the fit for  $\alpha$ -induced reaction on  $^{123}\text{Sb}$ . In general the agreement is reasonably good for most of the excitation functions for the theoretical calculation based on the hybrid model as described above for exciton values  $n_0=4$  ( $n_n=2$ ,  $n_p=2$ ,  $n_h=0$ ) and mfp multiplier parameter  $k=2.0$  in the range of energies these measurements are made. The theoretical values shown in the figures are multiplied by a factor so as to match the experimental data at the maximum cross-section point. The multiplying factors are given in figure captions. The multiplying factors also indicate the quality of fit between experimental and theoretical values. In general the hybrid model fits the excitation functions reasonably well, taking into account its limitations. Considering the multitudines of uncertainties in preequilibrium calculations such as (i) range of equilibrium and preequilibrium reaction cross section involved and (ii) in parameters such as inverse reaction cross sections and level densities, etc. Blann<sup>35</sup> considered that a result which is within a factor of 2 of the experimental result in absolute cross section and which generally has the correct spectral shape and variation of yield with excitation energy is an encouraging result.

However, there are a few exceptions:

(i) The fit shows a large discrepancy between theory and experiment for the reaction  $^{121}\text{Sb}(\alpha,2n)^{123}\text{I}$  at the high-energy tail side of the excitation function. This may be due to taking only one preequilibrium nucleon emission by the theory. With respect to preequilibrium reactions the program used can only account for the emission of a single nucleon. On the other hand, effects of preequilibrium emission of multinucleon and of complex particles were observed for the integral excitation functions<sup>39</sup> as well as for particle spectra.<sup>39,40</sup> However, there are no attempts published until now for the calculation of integral excitation functions with consideration of preequilibrium multinucleon and complex particle emission. So we are restricted to the analysis taking single preequilibrium nucleon emission only, whereas the excitation function shows clearly the emission of more than one preequilibrium nucleon.

(ii) The experimental excitation function for the reaction  $^{69}\text{Ga}(\alpha,2p4n)^{67}\text{Ga}$  has its maximum at the  $\cong 50$  MeV above which a pronounced plateau is seen. Here the theory fails completely to reproduce the experimental data. We guess that the high plateau cross section is produced by  $\alpha$  breakup into a  $^3\text{He}$  nucleus and a single neutron in the field of target nucleus. Such breakup phenomena have already been observed by Wu *et al.*<sup>41</sup> and also by Budzonowsky *et al.*<sup>42</sup> These authors observed considerable yields, for instance of  $^3\text{He}$  due to breakup of  $\alpha$  particles. Wu *et al.*<sup>43</sup> have demonstrated that an adequate description of the charged particle from the high-energy  $\alpha$  bombardment of  $^{27}\text{Al}$ ,  $^{58}\text{Ni}$ ,  $^{90}\text{Zr}$ ,  $^{209}\text{Bi}$ , and  $^{232}\text{Th}$  the breakup reaction mechanism is of great importance besides the compound-nucleus evaporation and the preequilibrium emission. These authors<sup>43</sup> found total yields of light particles which are by a factor of 2 or 3 larger than the total reaction cross section for light and medium weight target elements. Overlaid Alice,<sup>24</sup> on the other hand, does not account for the breakup of the projectile and preequilibrium emission of complex particles. However, at the moment it is not possible to decide from the known data whether the  $\alpha$ -particle breakup is in the field of the nucleus or whether the  $^3\text{He}$  is emitted really during the first step of the reaction which is ultimately leading to equilibrium. This point surely will deserve further investigation.

(iii) The large multiplying factor for  $^{121}\text{Sb}(\alpha,p3n)^{121}\text{Te}$  shows that the reaction mechanism is different from the one assumed for the calculation. We guess  $^{121}\text{Te}$  is produced by two different reactions, (a)  $^{121}\text{Sb}(\alpha,p3n)^{121}\text{Te}$  and (b)  $^{121}\text{Sb}(\alpha,4n)^{121}\text{I} \rightarrow (\beta^+) \rightarrow ^{121}\text{Te}$ , and what we measure is the sum of these two reactions. It is difficult to extract each contribution separately as the half-life of  $^{121}\text{I}$  is very short (2.12 h only).

## V. CONCLUSION

A consistent set of 13 excitation functions have been measured for  $\alpha$ -induced reactions on  $^{69}\text{Ga}$ ,  $^{71}\text{Ga}$ ,  $^{121}\text{Sb}$ , and  $^{123}\text{Sb}$  targets. The reliability of the cross sections were checked by intercomparison with other measurements of  $^{121}\text{Sb}(\alpha,2n)^{123}\text{I}$  (Ref. 25) and by comparing our

measurements of  $\alpha$ -induced reaction  $^{27}\text{Al}$  with other measurements<sup>18-26</sup> (see Sec. III E). Pronounced preequilibrium effects of nucleons have been observed for most of the reactions. From the reactions  $^{71}\text{Ga}(\alpha, 3n)^{72}\text{As}$  and  $^{123}\text{Sb}(\alpha, 3n)^{124}\text{I}$  an initial exciton number  $n_0=4$  ( $n_n=2$ ,  $n_p=2$ ,  $n_h=0$ ) with the mean-free-path multiplier parameter  $k$  set to 2 has been deduced for both the targets. The comparison of the experimental data with the results of the hybrid model calculations show a surprisingly good agreement without any parameter adjustment for individual products. Qualitatively, the model is able to reproduce the observed shapes reasonably well; quantitatively, the magnitude of the calculated cross section is, except for a few cases as mentioned above, within a factor of 2 and often closer than that to the observed cross sections over the entire energy range. Given the approximation inherent in the code, especially the limited treatment of the angular-momentum-dependent effects and neglect of the contributions from nonfusion processes, the agreement is as good as could be expected. By changing the values of the parameters it is possible to get a better account of the observed cross section as a function of the  $\alpha$  energy for a given product nucleus or for a broader range of product nuclei at a given energy, but always at a noticeable deterioration for other nuclei or other energies. Overall these comparisons confirm rather quantitatively that fusion evaporation (preequilibrium plus statistical) is the dominant mechanism. However, there are a few exceptions. The theory overestimates the cross section for the  $^{69}\text{Ga}(\alpha, 2p4n)^{67}\text{Ga}$  reaction whereas it underestimates the cross section for the  $^{121}\text{Sb}(\alpha, p3n)^{121}\text{Te}$  reaction and the high-energy tail of  $^{121}\text{Sb}(\alpha, 2n)^{123}\text{I}$  excitation functions. For the  $(\alpha, 2p4n)$  reactions on Ga the discrepancy between theory and experiment may be attributed partly to breakup of  $\alpha$  particle and partly to much more complex reaction mechanisms, whereas for the  $^{121}\text{Sb}(\alpha, p3n)^{121}\text{Te}$  reaction two different reaction mechanisms may be attributed. The large discrepancy between theory and experiment for the reaction  $^{121}\text{Sb}(\alpha, 2n)^{123}\text{I}$  at the high-energy tail of the excitation function may be attributed to emission of more than one preequilibrium nucleon which the theory cannot account for at present. Barring these reactions we have found the overall agreement between theory and experiment is reasonably good, taking the limitations of the theory into account. After taking these factors into account, we conclude that the dominant mechanism for the reaction induced by  $\alpha$  particle in the energy range of these measurements is fusion of the projectile and the target nuclei followed by decay of the resulting compound nucleus by preequilibrium and statistical evaporation.

#### ACKNOWLEDGMENTS

We wish to express our sincere thanks to Dr. B. C. Sinha, the director of the Variable Energy Cyclotron Centre (VECC), for his encouragements. We wish to thank the operational staff of the cyclotron for running the cyclotron smoothly during the experiments, the staff of IRIS-80 computer and ND-560 computer systems of

our centre for their assistance at various stages of calculation, and the target section for supplying the gallium and antimony targets in adequate numbers.

#### APPENDIX

The hybrid model for the preequilibrium reaction was proposed by Blann<sup>1</sup> and provides in some way a marriage between the simple exciton model proposed by Griffin,<sup>3</sup> and the more elaborate master equation approach due to Miller and co-workers.<sup>4,5</sup> Summarizing from Ref. 1, the main points of the hybrid model will be outlined here. As in high-energy cascade, it is assumed that the reaction proceeds through a series of particle-particle or particle-hole interactions, in which the total particle and hole numbers characterizing the nuclear state may either increase by two, decrease by two, or remain unchanged. It is assumed here that the transition in which the particle and hole (p-h) or exciton ( $n_e$ ) number increases by two dominates in the early stages of the equilibration process. As in Griffin's model, it is assumed also here that the intermediate states are characterized by appropriate level-density formulas and that all levels may be populated with equal *a priori* probability (within limitation of energy conservation and Pauli principle) during the equilibration process. As in earlier treatment of the exciton model, the total particle emission probability in a given channel energy range  $P_x(\epsilon)d\epsilon$  is given as a sum over the contributions of the intermediate states, although here this has significance as a statistical bookkeeping operation rather than an absolute time basis. The sum is taken from some initial number of excitons  $n_0$  to the equilibrium number  $n$ . The hybrid model predicts the probability of emission of a particle of type  $\nu$  in the channel energy range  $\epsilon$  to  $\epsilon+d\epsilon$  as

$$P(\epsilon)d\epsilon = \sum n P_\nu^* [N_n(\epsilon, u)/N_n(E)]^* g d\epsilon^* \\ \times \{ \lambda_c(\epsilon) / [\lambda_c(\epsilon) + \lambda_{n+2}(\epsilon)] \}^* D_n,$$

where  $nP_\nu$  is the number of particles of type  $\nu$  in an  $n$ -exciton state (where exciton number means the number of excited particles plus holes).  $N_n(\epsilon, u)$  is the number of ways  $n$  excitons can be arranged such that one exciton if emitted would have channel energy  $\epsilon$ , leaving a residual excitation of  $u = E - B_\nu - \epsilon$  distributed between other  $n-1$  excitons. The quantity  $N_n(E)$  represents a total number of combinations of  $n$  particles plus holes at excitation energy  $E$ . The quantity in the first set of square brackets represents the fraction of the  $n$ -exciton states having one exciton at energy  $\epsilon$  with respect to the continuum. The limiting value of the emission probability as defined by the above equation, integrated over all particle emission energy for a particular state with  $nP_\nu$  particle, is not unity but  $nP_\nu$ , i.e., the total number of excited particles.

Also in the above equation the emission rate into the continuum  $\lambda_c(\epsilon)$  of a particle at excitation  $\epsilon$  is given by

$$\lambda_c(\epsilon) = \sigma_\nu v \rho_c / g_\nu V,$$

where  $\sigma_\nu$  is the inverse cross section and  $v$  the velocity of

the particle having a density of states  $\rho$  in the continuum, and a single-particle density of state  $g_v$  in the nucleus;  $V$  is an arbitrary volume canceled by the same volume in  $\rho_v$ . The last factor  $D_n$  represents the fraction of the initial population surviving deexcitation by particle emission prior to the  $n$ -exciton state under consideration, i.e., the

prior decay depletion factor. The internal excitation rate  $\lambda_{n+2}(\epsilon)$  of an excited particle at energy  $\epsilon + B_v$ , above the Fermi energy has been based on the calculated mean free path in nuclear matter<sup>36</sup> which, however, can be calculated either from nucleon-nucleon scattering cross sections or from the imaginary part of the optical potential.<sup>8,9,35</sup>

<sup>1</sup>M. Blann, Phys. Rev. Lett. **27**, 337 (1971).

<sup>2</sup>C. K. Cline and M. Blann, Nucl. Phys. **A172**, 225 (1971).

<sup>3</sup>J. J. Griffin, Phys. Rev. Lett. **17**, 478 (1966).

<sup>4</sup>G. D. Harp, J. M. Miller, and J. B. Berne, Phys. Rev. **165**, 1166 (1968).

<sup>5</sup>G. D. Harp and J. M. Miller, Phys. Rev. C **3**, 1847 (1971).

<sup>6</sup>M. Blann, Annu. Rev. Nucl. Sci. **25**, 123 (1975).

<sup>7</sup>S. A. Hjorth, H. Ryde, K. A. Hagemann, G. Lovhoiden, and J. C. Waddington, Nucl. Phys. **A144**, 513 (1970).

<sup>8</sup>M. Ismail and A. S. Divatia, Bhabha Atomic Research Centre Report No. B.A.R.C./1366 (1987); and (unpublished).

<sup>9</sup>M. Ismail and A. S. Divatia, Pramana J. Phys. **30**, 193 (1988).

<sup>10</sup>M. Ismail, Pramana J. Phys. **32**, 605 (1988); Bhabha Atomic Research Centre Report No. B.A.R.C./1407 (1988).

<sup>11</sup>J. Ernst, R. Ibowski, H. Klampil, H. Machner, T. Mayer-Kuckuk, and R. Shanz, Z. Phys. A **308**, 301 (1982).

<sup>12</sup>C. Kaltach, Phys. Rev. C **23**, 124 (1981).

<sup>13</sup>M. L. Goldberger, Phys. Rev. **74**, 1268 (1948).

<sup>14</sup>C. J. Mathews, B. G. Glagola, R. A. Moyle, and V. E. Voila, Jr., Phys. Rev. C **25**, 2181 (1982).

<sup>15</sup>R. Serber, Phys. Rev. **72**, 1114 (1947).

<sup>16</sup>I. Dostrovsky, Z. Frankel, and G. Friedlander, Phys. Rev. **116**, 683 (1959); **118**, 781 (1960); **118**, 791 (1960).

<sup>17</sup>F. Puhlhofer, Nucl. Phys. **A280**, 267 (1977).

<sup>18</sup>H. J. Probst, S. M. Qaim, and R. Weinreich, Int. J. Appl. Radiat. Isot. **27**, 431 (1976).

<sup>19</sup>C. F. Williamson, J. P. Boujot, and J. Picard, Commissariat à l'Energie Atomique (France) Report No. CEA-R 3042 (1966).

<sup>20</sup>J. Kern (unpublished).

<sup>21</sup>J. Kern, Nucl. Instrum. Methods **79**, 233 (1970).

<sup>22</sup>C. M. Lederer and V. S. Shirley, *Table of Isotopes, 7th Edition* (Wiley, New York, 1978).

<sup>23</sup>A. H. Wapstra and G. Audi, Nucl. Phys. **A432**, 1 (1985).

<sup>24</sup>M. Blann, University of Rochester Report No. Coo-3494-29,

1975 (unpublished).

<sup>25</sup>A. Colboreanu, P. Constanin, and O. Salageon, Nucl. Phys. **A383**, 251 (1982).

<sup>26</sup>J. Jastrzebski, P. P. Singh, T. Mroz, S. E. Vigdor, M. Fatya, and H. J. Karwowski, Phys. Rev. C **34**, 60 (1986).

<sup>27</sup>R. Birkelund, L. E. Tubbs, J. R. Huizenga, J. N. De, and D. Sperber, Phys. Rep. **56**, 108 (1979).

<sup>28</sup>E. Gadioli and E. Gadioli-Erba, Nucl. Instrum. Methods **146**, 265 (1977).

<sup>29</sup>A. Mignerey, M. Blann, and W. Scobel, Nucl. Phys. **A273**, 125 (1976).

<sup>30</sup>H. C. Chiang and J. Hufner, Nucl. Phys. **A349**, 466 (1980).

<sup>31</sup>V. F. Weisskopf and D. H. Ewing, Phys. Rev. **57**, 472 (1940).

<sup>32</sup>W. D. Mayers and W. J. Swiatecki, Nucl. Phys. **81**, (1966).

<sup>33</sup>W. D. Mayers and W. J. Swiatecki, Ark. Fys. **36**, 343 (1967).

<sup>34</sup>F. D. Becchetti and F. D. Greenlees, Phys. Rev. **182**, 1190 (1969).

<sup>35</sup>M. Blann, Nucl. Phys. **A213**, 570 (1973).

<sup>36</sup>K. Kikuchi and M. Kawai, *Nuclear Matter and Nuclear Reaction* (North-Holland, Amsterdam, 1968).

<sup>37</sup>M. Blann and A. Mignerey, Nucl. Phys. **A186**, 245 (1972).

<sup>38</sup>E. Gadioli, E. Gadioli-Erba, L. Sajo-Bohus, and G. Tagliaferri, Rev. Nuovo Cimento **6**, 1 (1976).

<sup>39</sup>E. Gadioli, E. Gadioli-Erba, and J. J. Hogan, Phys. Rev. C **16**, 1404 (1977).

<sup>40</sup>A. Chevarier, N. Chevarier, A. Demeyer, G. Hollinger, P. Pertosa, and T. M. Duc, Phys. Rev. C **8**, 2155 (1973).

<sup>41</sup>J. R. Wu, C. C. Chang, and H. D. Holmgren, Phys. Rev. Lett. **40**, 1013 (1978).

<sup>42</sup>A. Budzanowski, G. Baur, C. Alderlisten, J. Bojawald, C. Mayer-Böricke, F. Rösler, and D. Trantmann, Phys. Rev. Lett. **41**, 635 (1978).

<sup>43</sup>J. R. Wu, C. C. Chang, and H. D. Holmgren, Phys. Rev. C **19**, 659 (1979).